Standardizing the Mode I Fatigue Delamination Growth Tests for Fibre Reinforced Polymer Composites

Master of Science Thesis

Aditya Muralidharan

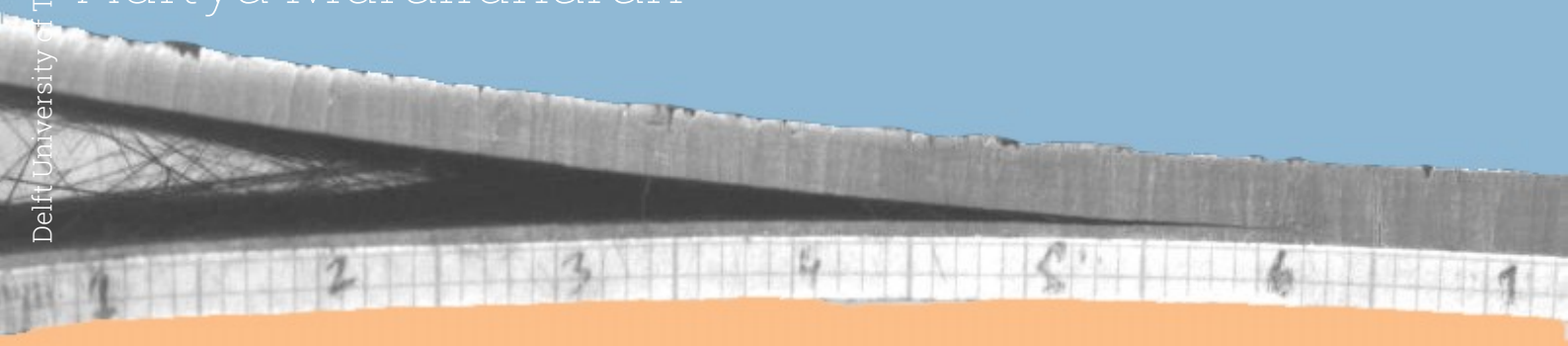

Delft University of Technology

TU Delft

Standardizing the Mode I Fatigue Delamination Growth Tests for Fibre Reinforced Polymer Composites

by

Aditya Muralidharan

to obtain the degree of Master of Science
at the Delft University of Technology,
to be defended publicly on Friday November 22, 2024 at 10:00 AM.

Student number:	5709504
Project duration:	February, 2024 – November, 2024
Thesis committee:	Dr. Rene Alderliesten
	Dr. Rinze Benedictus
	Dr. Calvin Rans

Cover:	Fibre Bridging Observed By Rafiullah Khan[1]
Style:	TU Delft Report Style, with modifications by Daan Zwaneveld

An electronic version of this thesis is available at http://repository.tudelft.nl/.

TU Delft

Copyright © Aditya Muralidharan, 2024
All rights reserved.

Abstract

Fibre-reinforced polymer (FRP) composites have become indispensable in aerospace engineering over the past two decades, driving the need for efficient and standardized testing protocols to certify their reliability. However, no standardized protocol currently exists for fatigue testing of FRPs, particularly due to fibre bridging—a phenomenon prominent in testing but rarely encountered in real-world applications. This study investigates existing fatigue data processing techniques, with a primary focus on a regression-based approach that could standardize fatigue data analysis.

Current fatigue delamination characterization methods often rely on single-parameter empirical models, which struggle to capture the complex interaction between cyclic and monotonic load components, expressed as $\Delta\sqrt{G}$ and G_{max}, respectively. This study demonstrates that the regression method's zero-bridging technique effectively incorporates both parameters, offering a comprehensive view of delamination growth by isolating it from fibre bridging effects. This approach suggests a shift away from the traditional 2D analysis to a 3D framework, which considers both G_{max} and $\Delta\sqrt{G}$, enabling a more accurate depiction of delamination behavior across various stress ratios. Notably, the results reveal that zero-bridging data align on a common plane under consistent stress ratios, shifting as stress ratios increase. Additionally, fiber orientation influences data clustering, with similar orientations exhibiting stronger convergence than dissimilar ones.

Comparison of this regression-based method with the modified Paris law reveals significant discrepancies in its current implementation, suggesting alternative approaches to address these limitations. This study also highlights the impact of data size and selection on the model behavior, stressing their importance in accurate model representation. This research validates the regression method as a promising candidate for standardizing fatigue data processing, improving the precision and reliability of post-test analysis for fibre-reinforced polymer composites.

Contents

Nomenclature

Abbreviations

Abbreviation	Definition
CFD	Crack Driving Force
CFRP	Carbon Fibre Reinforced Polymer
CFD	Cumulative Distribution Function
CC	Compliance Calibration
DCB	Double Cantilever Beam
FRP	Fibre Reinforced Polymer
FAA	Federal Aviation Authority
GFRP	Glass Fibre Reinforced Polymer
LEFM	Linear Elastic Fracture Mechanics
MBT	Modified Beam Theory
MCC	Modified Compliance Calibration
SIF	Stress Intensity Factor
SERR	Strain Energy Release Rate

List of Figures

1

Introduction

The use of composites for aircraft primary structures dates back to 1984 when it was used in the Boeing 737 horizontal tail[2]. This structure was certified by the Federal Aviation Authority using the Airworthiness Advisory Circular 20-107A in 1984. This certification was carried out based on the use of a test based no-detrimental damage growth philosophy which closely resembles the safe life methodology in its metallic counterparts.

This has paved the way for the use of composites structures on aircrafts such as the Boeing 787 Dreamliner[3] and the Lockheed Martin F-35A[4] where they are composed almost entirely of composite skins which has resulted in a 30-40% ratio of composite structures to aircraft weight. Even though multiple decades have passed, aircrafts such as the Boeing 787 are still lifed under the same no-detrimental growth philosophy which works based on physical testing.

This conservative design philosophy, while effective in ensuring structural safety, has led to significant expenditure on structural testing. The need for such conservative measures has, in turn, resulted in thicker composites, ultimately increasing aircraft weight. In 2009, the FAA updated its guidelines[5] to allow for the use of damage-tolerant systems, provided the anticipated damage remains slow, stable, and predictable throughout the structure's service life. This update has spurred extensive research into understanding and managing fatigue damage growth, aiming to optimize structural design without compromising safety.

Given the rigorous certification requirements in order to avoid catastrophic failures the safety and reliability of the composites need to be studied extensively. Composites are susceptible to various modes of damage like fibre breakage, matrix cracking, delamination between adjacent layers etc. This, coupled with the interaction between different damage modes, makes characterizing damage evolution very difficult. Past research has resulted in a common consensus that delamination was the most important damage mechanism in composite laminates and plays a crucial role in structural design when using composites[6]. This delamination can

be caused due to stress concentrations and poor interlaminar properties of the material. Delamination and delamination propagation can easily be caused by to lack of reinforcement in the thickness direction between adjacent layers. Specifically, under fatigue loading this delamination can propagate causing gradual degradation in strength and stiffness finally resulting in the catastrophic failure of the composite structures in their service lives.

With safety factors and tolerance being an important part of any design process the need to characterize fatigue delamination for composite laminates becomes a necessity. Pascoe[6] stressed that the methods based on fracture mechanics were influential in characterizing delamination growth. With this framework as the base, stress intensity factor (SIF) and strain energy release rate (SERR) can be used to determine the crack growth. The Paris relation has been widely used in designs and studies over the last several decades even though it has been a common consensus amongst researchers that it is nothing more than an empirical correlation and is not based on physical understanding of fatigue delamination growth[6]. The lack of a consensus in a similitude parameter for fatigue delamination studies resulted in the use of either the maximum SERR G_{max}, The SERR range ΔG, or a combination of both to determine fatigue crack growth[7–11].

A valid crack driving force (CDF) is needed for the 'similitude hypothesis' to be applicable[12]. In the case of metals, this is more straightforward as the range in the applied stress intensity factor, ΔK is used as the CDF. In order to define a 'similitude principle' for composites it's important to start with understanding what exactly the similitude principle in this context indicates. In the case of metals, the basic 'similitude hypothesis' is expressed as:

"Two different cracks growing in two different specimens of the identical material with the same thickness and the same CDF, and with the same value of K_{max}, will grow at the same value of da/dN."

This definition cannot be directly applied to composites using the same or similar parameters, as their behaviour is more complex than that of metals. Similar to the case of metals the delamination growth is experimentally observed to have a linear relationship with the different formulations of the SERR when plotted on the log-log scale. This results in a consensus on the overall formulation of the delamination growth as a function of the SERR, *f(G)* but there is no consensus on the term that can be used to define it. The most prominent formulations of the *f(G)* are G_{max} [13, 14] whose use is analogous with the static delamination growth and ΔG which is believed to be the equivalence of the ΔK that is used in the case of the metals. A major issue highlighted in the literature regarding this approach is that it relies solely on curve fitting through experimental data, without offering a physical explanation for the observed behaviour.

Another major obstacle in the standardization process is the concept of fibre bridging. Fibre bridging is an important shielding mechanism that is exhibited where the bridging fibres increase the interlaminar resistance by restraining the crack opening during crack extension[15–17]. The issue that arises in the case of fibre bridging is the fact that this phenomenon is observed only within the concept of testing and is very rarely seen in real operational conditions.

As fibre bridging is known to enhance the toughness of the composite and slow down the delamination process it becomes imperative that this phenomenon be accounted in order to avoid under designed composite structures.

There have been prediction models that have been developed assessing the contribution of this effect to the crack growth[18, 19] in the case of quasi-static crack growth, but this does not translate to the fatigue delamination growth. Similar to the previous case, the models that were proposed in order to account for fibre bridging were empirical curve fits to the data and did not have a physical basis for them.

1.1. Thesis Outline

The literature review is presented in chapter 2, summarizing the existing methods and considerations relevant to this study. The research objective and the research questions are presented in chapter 3. The methodology is outlined in chapter 4, detailing the calculations and plotting techniques employed to analyze the proposed methods. chapter 5 presents the results and discussions, starting with observations from the method and its validation. This is followed by a comparison of the regression method with the modified Paris relation, highlighting the strengths and limitations of both approaches. The conclusions and future work recommendations are provided in chapter 6 and chapter 7, respectively. Additionally, Appendix A includes the plots of unsuccessful plane-fitting attempts.

2

Literature

There is a common tendency to treat the different fibre reinforced composites as though they were metals. When the concept of fatigue was adapted from metals to composites, a similar model was initially applied, assuming a single crack that progressively grows with each fatigue cycle. However, crack growth in composites is far more complex due to the interactions between different plies, leading to intricate damage mechanisms. It was once believed that composite structures would not fail under cyclic fatigue loading if the applied load remained below the material's maximum stress[20]. Because of their high fatigue resistance, composites were thought not to exhibit traditional fatigue crack growth behaviour. This idea was supported by the assumption that the high stiffness in the fibre direction could prevent the strain levels needed for damage initiation, which could be controlled through careful design modifications.

This assumption resulted in the over-designing of the structures which in turn resulted in increased weight and costs. The anisotropic behaviour exhibited by composites also meant that small out-of-plane loads or strains could initiate damage, ultimately resulting in failure. This highlights the importance of studying damage growth in fibre-reinforced polymers (FRPs), especially in aerospace applications, where understanding these mechanisms is critical to ensuring structural integrity and optimizing design.

2.1. Fatigue in Composites

To characterize fatigue in composites, it is essential to understand the mechanisms of delamination growth under cyclic loading. In composites, a pre-existing crack may or may not propagate under cyclic loading, depending on the material's specific properties. Over time, accumulated damage can reduce the composite's residual load-bearing capacity to the point where it falls to the maximum stress level of the fatigue cycle, as shown in Figure 2.1. Predicting fatigue life in composites is complex due to the interaction of various damage mechanisms. One approach to assess fatigue life is through the S-N curve, which relates cyclic stress to the

number of cycles to failure. Unlike metals, composites often lack a clear fatigue limit, allowing damage to accumulate even under low-stress conditions.

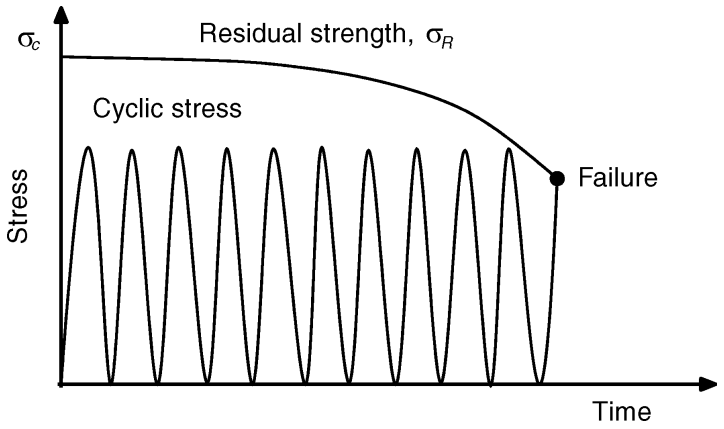

Figure 2.1: Degradation of composite strength until residual strength reaches maximum stress of the fatigue cycle

When looking at delamination growth under fatigue loading it is important to understand how fatigue works. During each cycle, the stress alternates between S_{max} and S_{min}, passing through S_{mean} as seen in Figure 2.2.

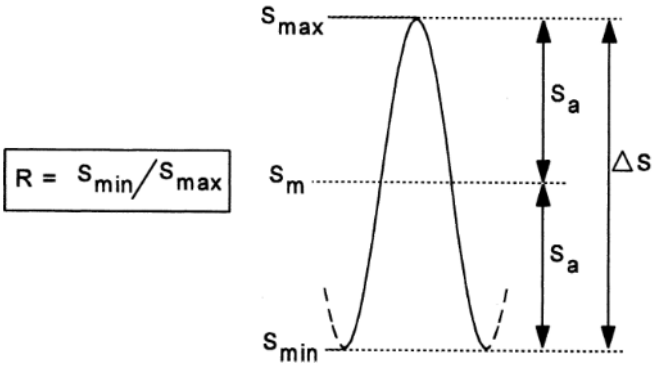

Figure 2.2: Fatigue Cycle[21]

This proposed delamination growth can occur in various modes: mode I (tensile), mode II (shear), mode III (transverse shear) or mixed mode, which combines these different modes.

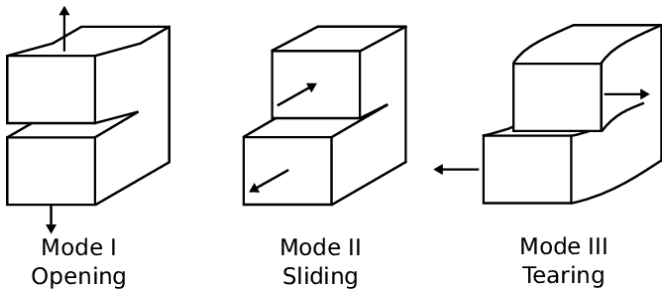

Figure 2.3: Different Modes of Delamination Growth

The focus of this thesis is on mode I fatigue delamination. Fatigue delamination growth under mode I occurs exclusively under tension loading, as the crack remains closed under mode I compression, preventing any delamination growth. This cyclic loading can result in delamination growth in composites particularly in regions where the stress ratio (the ratio of minimum stress to maximum stress, R = S_{max}/S_{min})is between -∞ and 1. as seen in Figure 2.4. In the tension-compression region, delamination primarily grows during the tension portion of the cycle, as the compression portion typically closes the crack, preventing growth. When the stress ratio R is 0, it indicates that the minimum stress is zero, meaning the material is fully relaxed during the compression part of the cycle.

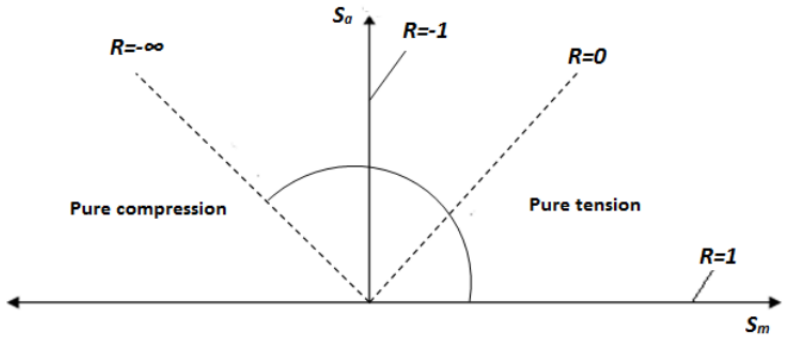

Figure 2.4: Stress ratio relation under Mode I[21]

2.2. Damage Tolerance in Composites

As discussed in chapter 1, composite structures can be certified using one of two main philosophies: damage tolerance or safe life. The safe life approach has traditionally been the more widely used method, as it requires less complex analytical work and focuses heavily on extensive testing. This testing regimen is designed to demonstrate conclusively that the component will not sustain damage throughout its entire operational lifespan, ensuring the structure remains free from cracks or damage during service. However, the extensive time and high costs associated with such testing have driven interest toward an alternative approach: damage tolerance.

The damage tolerance philosophy, often associated with the ”slow growth” concept, is particularly suitable for designing lighter structures. This approach accommodates the controlled and predictable progression of damage, such as fatigue-induced cracks, allowing for the design of components that can endure limited damage growth. For damage tolerance to be effective, the damage mechanisms must be thoroughly understood so that inspections can be strategically planned to detect and mitigate critical damage before it compromises structural integrity.

In metallic structures, damage progression in Mode I typically occurs perpendicular to the loading direction. However, in composites, failure follows a more complex network of mechanisms, often running parallel to the load axis. This emphasizes the need for both qualitative and quantitative understanding of interactions under fatigue loading, making accurate prediction of the

behaviour challenging. This lack of comprehensive understanding leads to composite structures being consistently over sized for aerospace applications, thereby diminishing the cost benefits that composites are supposed to provide compared to traditional metal structures.

2.3. Delamination Growth Prediction Methods

The Paris relation is frequently utilized to describe the fatigue crack growth rate, though it remains a largely empirical formula. Prediction models for characterizing fatigue crack growth are categorized into four primary types [6]:

- Stress/strain-based methods
- Fracture mechanics-based methods
- Cohesive zone models
- Extended finite element models

Stress/strain methods have traditionally been applied to model the strength and fatigue life of adhesive bonds and metal structures[22]. This approach evaluates the stress and strain fields within materials and their response to applied loads, aiming to predict failure under these conditions. However, this method is less effective for modeling delamination growth in fibre-reinforced polymer (FRP) composites due to its inability to capture the complexities involved in the delamination process adequately. These methods are typically employed in static delamination problems where the focus is on determining fatigue life rather than tracking delamination growth[6]. Furthermore, these methods do not provide detailed insights into the rate and progression of delamination growth under cyclic loading, which is a common scenario for FRPs in practical applications.

2.3.1. Linear Elastic Fracture Mechanics

Linear elastic fracture mechanics involve the use of stress intensity factor (SIF) and strain energy release rate (SERR) to model the growth of delamination under fatigue loading. It is essential to understand that these two parameters are interchangeable, as neither provides more or different information than the other. When it comes to composite materials, using the Stress Intensity Factor (SIF) to characterize delamination growth presents significant challenges. The primary difficulty lies in the complex stress fields at the delamination front of orthotropic materials, making SIF analysis inconvenient and less effective for these materials. In contrast, the use of Strain Energy Release Rate (SERR) has proven to be a more effective and practical alternative for analyzing delamination growth. Consequently, SERR has become widely adopted for characterizing delamination behaviour in composite materials. The use of fracture mechanics in fatigue characterization is not novel and dates back to Paris who proposed his relation where he related the delamination growth rate as a function of the SIF. In it's most basic form it is written as:

$$\frac{da}{dN} = C\Delta K^n \tag{2.1}$$

where the terms C and n are curve fitting parameters making the Paris relation an empirical relation that is modified in order to provide the best curve fit. This was later written using SERR instead but the major issue lied in the lack in consensus over the choice of the parameter that was used. The general form of the relation written in terms of the SERR is as follows:

$$\frac{da}{dN} = Cf(G)^n \tag{2.2}$$

where $f(G)$ is a parameter that is a function of G.

2.3.2. Crack Driving Force in Composites

The certification process for composite structures using the slow crack growth methodology requires that the lifing approach be both gradual and predictable. To achieve accurate predictions, testing must effectively characterize the material's slow crack growth behaviour under specific geometries and loading conditions, a concept referred to as the similitude parameter. Following the concepts of Linear Elastic Fracture Mechanics (LEFM) in metals, this similitude parameter is well-established as the Stress Intensity Factor range, $\Delta K = K_{max} - K_{min}$, which is plotted against the crack growth rate, da/dN, to produce a distinct fatigue crack growth curve. For a given material, the crack growth rate corresponding to a particular Stress Intensity Factor remains consistent, ensuring reliable predictions.

When applying this concept to composites, the focus shifts to the Strain Energy Release Rate (SERR), which is analogous to the Stress Intensity Factor (SIF) in metals. In composites, the stress intensity factor (SIF) range was adapted to the strain energy release rate (SERR) range, defined as $\Delta G = G_{max} - G_{min}$, or simply as the maximum SERR, G_{max}. The SERR can be calculated using the following equation:

$$G = \frac{1}{2t} P^2 \frac{dC}{da} \tag{2.3}$$

Here, P represents the applied load, t is the thickness, C is the compliance, and a is the crack length. The maximum and minimum values of SERR can be determined by substituting the maximum and minimum forces for P.

However, it has been found that SERR is less effective as a similitude parameter in composites. This ineffectiveness can be attributed to the noticeable reduction in SERR when the R-ratio is increased. Moreover, the behaviour of delamination growth varies depending on which parameter is used: when G_{max} is employed, delamination growth decreases with an increased R-ratio, while the opposite trend is observed when using ΔG as observed by Rans et al. [23].

This observation led to further research, revealing that the term G used in the SERR formu-

lation is actually proportional to K^2, the square of the Stress Intensity Factor. This discovery resulted in the development of a more accurate similitude parameter related to $\Delta\sqrt{G}$, which is defined as $(\sqrt{G_{max}}-\sqrt{G_{min}})^2$. This parameter provided a better correlation for characterizing crack growth in composites, aligning more closely with the behaviour observed in the materials under varying conditions. The other issues highlighted in previous studies [24] appeared to be mitigated when applying the new formulation within the modified Hartman-Schijve equation Equation 2.4:

$$\frac{da}{dN} = D\left[\frac{\Delta\sqrt{G}-\Delta\sqrt{G_{thr}}}{\sqrt{1-\sqrt{G_{max}/\sqrt{A}}}}\right]^n \tag{2.4}$$

In this equation, $\Delta\sqrt{G} = (\sqrt{G_{max}}-\sqrt{G_{min}})^2$, and G_{thr} can be derived from the R-curve. Jones et al. [25, 26] asserts that using Equation 2.4 produces a curve that is independent of variables such as material thickness, temperature, R-ratio, pre-crack length, ply configuration, laminate, and adhesive thickness. This independence facilitates a more accurate analysis of delamination growth in composites.

2.3.3. Stress Ratio Dependence

As mentioned previously, there is no consensus on whether the Paris relation should be a function of G_{max} or ΔG. Historically, the choice of parameter to characterize delamination growth depended on the researcher's understanding and convenience, with no established standard enforcing the use of a specific parameter. While modeling delamination growth a key parameter that needs to be considered is the stress ratio, R. The stress ratio is defined as the ratio of the minimum stress to the maximum stress in a fatigue cycle. Experimental evidence suggests that this parameter has a significant influence on the growth of delamination in composites[10, 21].

Different definitions of $f(G)$ have been considered when modeling delamination growth using Equation 2.2, including G_{max}, $\Delta G = G_{max} - G_{min}$, and $\Delta\sqrt{G} = (\sqrt{G_{max}}-\sqrt{G_{min}})^2$. The primary issue with using these parameters is that the exponent parameter often becomes too large, leading to significant uncertainties in predicted delamination growth due to small uncertainties in the applied loading[27]. The influence of the stress ratio on the delamination growth is evident when plotting the Paris relation with with the maximum SERR or the SERR range as seen in Figure 2.5. This influence can be characterized by a shift in the position of the curves. The observed trend is an increase in the da/dN values as the R-ratio is increased for the same cyclic load[28].

Researchers have explored various definitions of the strain energy release rate (SERR) to characterize delamination growth in fibre-reinforced composites. When plotting data using both the SERR range and the maximum SERR, a common observation emerged: using G_{max}

to plot different R ratios revealed a clear distinction between the curves. However, this distinction was not observed when using the SERR range ($G_{max} - G_{min}$)[29, 30]. Similar behaviour was reported by Mall et al. [31] in bonded structures. Additionally, Rans et al. [23] noted that when plotting $G_{max} - G_{min}$, an increasing R ratio (and thus increasing the mean or peak stress) resulted in a decrease in the growth rate for the same cyclic conditions. This behaviour was attributed to the fact that for a constant $\Delta G = G_{max} - G_{min}$, both cyclic and monotonic loading conditions change to preserve ΔG with varying R ratios. This paper later goes on to highlight that the use of $\Delta G = G_{max} - G_{min}$ in the is used in a form analogous to ΔK but the definition of SERR range that uses the same basis for similitude as ΔK was $\Delta\sqrt{G} = (\sqrt{G_{max}} - \sqrt{G_{min}})^2$. This also reduced the mean load dependency that was present when $\Delta G = G_{max} - G_{min}$ was used.

In more recent studies using a two-parameter model, Khan et al. [1] noted that the cause of the stress ratio effect remained unclear. He emphasized that the similitude parameters were not well-conceived, with the representation largely constrained to a two-dimensional representation. This representation was often based either on the monotonic load component, G_{max}, or the cyclic load component, $\Delta\sqrt{G}$. Khan's findings led to the hypothesis that another phenomenon or mechanism might be responsible for the observed stress ratio effect. It was further argued that the cyclic application of load, followed by the specimen's deflection, suggests the presence of cyclic energy. Since this cyclic energy is observed to vary with the stress ratio, it is reasonable to expect that this variation would be reflected in the delamination resistance results.

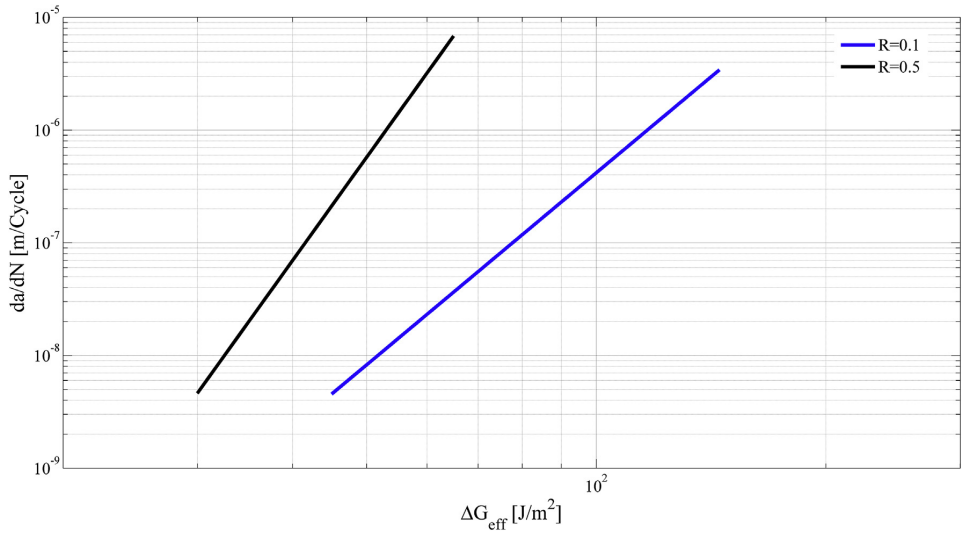

Figure 2.5: R-ratio effect as observed by Yao et al.[32]

2.4. Two-Parameter Models

Attempts were made to explain the effect of the R-ratio that was discussed in the previous section and the most prominent approach that was followed was the two-parameter model. This methodology revolved around the common belief that a single parameter cannot fully

describe fatigue crack growth[1, 30, 33–38]. A similar issue as before was faced as there was no physical explanation provided for the effect with most of the proposed models being curve fits through empirical data. Under constant amplitude loading a fatigue cycle can be described by both cyclic and monotonic load components as shown in Figure 2.6. These components can be P_{max} and ΔP, P_a and P_m (where P_a is the amplitude load and P_m is the mean load), or ΔP and the stress ratio R. This is analogous with the idea that two parameters are required to properly describe a fatigue cycle.

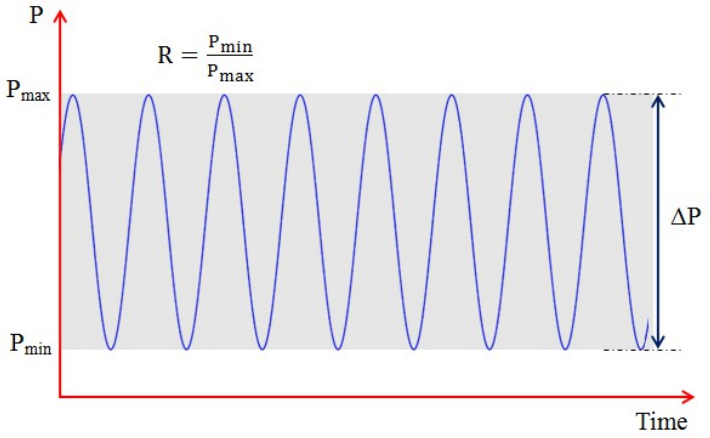

Figure 2.6: Constant Amplitude Fatigue Load

The initial efforts to implement the two-parameter model concentrated on the use of the Stress Intensity Factor (SIF), incorporating both ΔK and K_{max}. Hojo et al. [10] established an empirical relationship for this purpose, expressed as:

$$\frac{da}{dN} = c(\Delta K)^{(1-\gamma)n} K_{max}^{\gamma n} \tag{2.5}$$

In this context, γ serves as a material parameter that reflects the relative influence of the loading parameters. Its value ranges from 0 to 1: when γ is closer to 1, the crack growth rate is predominantly influenced by K_{max}, whereas when γ is closer to 0, ΔK becomes the dominant factor. The application of SIF in this equation is consistent with its role as a similitude parameter in the fatigue analysis of metals.

Jia et al. [36] expanded on Hojo's approach by extending it to the Strain Energy Release Rate (SERR), proposing an equivalent SERR term, G_{eq}. Different formulations of this term were explored, leading to the development of the following equation:

$$\frac{da}{dN} = B(\Delta G^{(1-\gamma)} G_{mean}^{\gamma})^m \tag{2.6}$$

Here, B and m are curve-fitting parameters, and the equation is another empirical fit. Note must be taken for the fact that the definition of ΔG in this equation parallels that of ΔK in Equation 2.5.

Atodaria et al. [35] proposed a similar two-parameter model, but utilized $(\sqrt{G})_{average}$ instead of G_{max}. The term $(\sqrt{G})_{average}$ is defined as:

$$\left(\sqrt{G}\right)_{\text{average}} = \left[\frac{1}{n}\sum_{\sqrt{G_{\text{th}}}}^{\sqrt{G_{\text{max}}}}\left(\sqrt{G}\right)^{w}\right]^{1/w} \tag{2.7}$$

In this equation, n represents the number of divisions between the maximum and threshold values, and w is a weighting factor. This weighting factor revolves around that idea that the process of fatigue crack growth is gradual with variations as stresses move between minimum and maximum. This means that a lower growth rate is observed at lower stresses an vice versa. However, the main limitation of Atodaria's model was its reliance on five equation parameters that had to be determined iteratively, making it cumbersome and complex.

Building on the insights proposed by Rans et al. [23] regarding the appropriate translation of SERR from SIF, the original equation proposed by Hojo can be reformulated as:

$$\frac{da}{dN} = c(\sqrt{G_{max}} - \sqrt{G_{min}})^{2(1-\gamma)}G_{max}^{\gamma n} \tag{2.8}$$

Although the proposed equations are empirical, a consistent trend among them is their foundation in linear elastic fracture mechanics. One of the more recent models proposed by Khan et al. [37, 38] was a mechanistic approach that involved the use of fractography to correlate the monotonic and cyclic part in the form of G_{max} and ΔG and the relation is given as seen in Equation 2.9 where the terms A, B, n and m are obtained from the SEM observations.

$$\frac{da}{dN} = A(G_{max})^{m} + B(\Delta G)^{n} \tag{2.9}$$

Yao et al. [39] proposed another two-parameter model to investigate the effects of temperature and stress ratios on fatigue delamination behaviour. This model extends the modified Paris relation previously introduced by Yao et al. [40], but it utilizes $\Delta\sqrt{G_{tip}}$ and G_{max_tip} as the two parameters. The resulting equation is expressed as follows:

$$\frac{da}{dN} = C\left(\Delta\sqrt{G_{\text{eff}}}\right)^{n} = C\left[\Delta\sqrt{G_{\text{tip}}}\left(1-\left(\frac{G_{\text{max\_tip}}}{G_{IC0}}\right)^{\gamma}\right)\left(\frac{G_{\text{max\_tip}}}{G_{IC0}}\right)^{\gamma}\right]^{n} \tag{2.10}$$

In this equation, G_{max_tip} represents the maximum Strain Energy Release Rate (SERR) at the delamination front, and γ is the weighting parameter. The value of G_{max_tip} can be calculated using the following formula:

$$G_{max\_tip} = \frac{\Delta\sqrt{G_{tip}}}{(1-R)^2} \tag{2.11}$$

This formulation allows for the consideration of the combined effects of temperature and stress ratios on the fatigue delamination process, offering a more comprehensive understanding of the behaviour under varying conditions.

The main takeaways from the analysis of the two-parameter models that are proposed is that the R-ratio effect seems to disappear when analysing experimental data. The empirical nature of the proposed relations results in differences in the damage mechanisms that are followed under monotonic and cyclic loading. This makes the product of the G_{max} and ΔG a questionable choice. The γ term in the equation proposed by Hojo presented an issue, as it was not constant for the same material and was dependent on the crack growth rate[41]. Khan et al. [1] pointed out that the discrepancies with the model that was proposed by Hojo was more evident at high crack growth rates. Despite the issues related to the proposed models, the two-parameter models are essential for understanding the individual contributions of the monotonic and cyclic parts of the fatigue cycle.

2.5. Effect of Fibre Bridging

Fibre Bridging acts as a shielding mechanism that can span fracture surfaces and inhibit crack growth. This shielding mechanism is observed at the crack tip resulting in a reduced stress intensity thereby inhibiting crack propagation. As the Double Cantilever Beam used in tests are unidirectional, the presence of nesting fibres between adjacent plies results in fibre bridging at the interface.

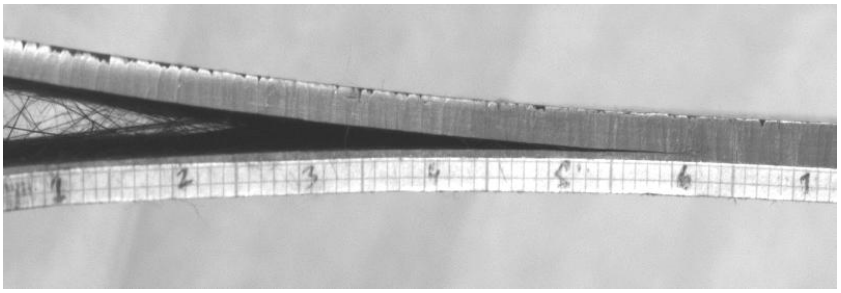

Figure 2.7: Bridging fibres during a DCB test [1]

Fibre bridging is known to enhance the toughness of the composite and can significantly slow down the delamination process[15–17]. Furthermore, this phenomenon is observed only in the context of the DCB tests that are performed and are very rarely seen in operation of real structures[42]. During quasi-static delamination, the fracture resistance initially increases eventually reaching a plateau due to fibre bridging behind the crack front. This behaviour can be observed by the means of plotting an R-curve which represents the relation between the crack length and fracture resistance. The plateau that is reached towards the end of the R-curve marks the end of the development of bridging fibres.

Fibre bridging in composites has been extensively studied, with a primary focus on understanding the conditions under which delamination growth occurs. Fibre bridging enhances

the fracture toughness of composite materials; however, since crack growth behaviour is influenced by this phenomenon, its characterization is crucial. Early research attempted to quantify the effect of fibre bridging by physically severing the bridged fibres and subsequently subjecting the material to fatigue loading. This approach demonstrated an increase in delamination growth after cutting the bridged fibres[43]. Further studies revealed that the density of bridged fibres varies along the crack length, with a higher density near the crack tip, which diminishes with increasing distance from the tip[44]. This variation can be attributed to the detachment or fracture of fibres, which no longer contribute to the bridging effect.

The influence of fibre bridging is effectively illustrated through resistance curves. Yao et al. [40] demonstrates this relationship, as shown in Figure 2.8. As the pre-crack length increases, the resistance curve shifts to the right. When the pre-crack length surpasses a certain threshold, the resistance curves converge, indicating that fibre bridging has fully developed.

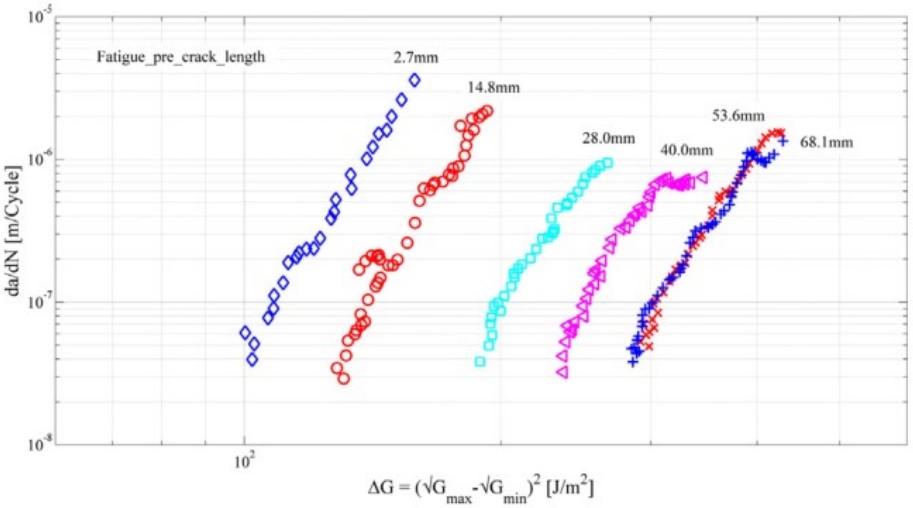

Figure 2.8: Fibre bridging effect in resistance curves[40]

Modeling delamination growth with fibre bridging introduces additional complexity, as the extent of fibre bridging is highly variable and challenging to accurately capture or standardize. Initial studies revealed that traditional Linear Elastic Fracture Mechanics (LEFM) methods were inadequate for accurately capturing fibre bridging effects, underscoring the need for more advanced models capable of representing this behaviour comprehensively. Several factors influence the extent of fibre bridging, leading to inconsistencies in test results, which further complicates the establishment of a standardized testing protocol.

Most research on fibre bridging has been predominantly phenomenological, with limited grounding in fundamental physics. This lack of a robust physical foundation becomes apparent when performing a dimensional analysis on the proposed equations[45]. Without a well-established similitude parameter to accurately represent delamination growth under fatigue loading, many approaches have relied on the stress intensity factor (SIF), a concept adapted from quasi-static testing and fatigue growth behaviour in metals. While this approach offers some insights, it

does not fully capture the complexities of delamination growth in fibre-reinforced composites.

Yao[46] investigated the underlying physics of fatigue delamination, observing that the energy released during the process remains largely constant. He noted that while energy is stored and released by the bridging fibres, it only contributes to the total energy released if the fibres fail. Alderliesten[45] highlighted the importance of developing a predictive model based on the crack driving force (CDF), rather than focusing solely on the consequences of crack growth. Building upon these insights and scanning electron microscopy (SEM) observations of fracture surfaces, Yao[40] proposed the use of the strain energy release rate that is applied directly to the crack tip as the crack driving force in fatigue delamination with fibre bridging.

This concept was initially explored by Jones[47] as an extension of the Hartman-Schijve equation, utilizing the J-integral method to determine the threshold SERR. The J-integral method, originally proposed by Suo[48], divides the total SERR around the crack front into the SERR at the crack tip and the SERR contributed by the bridging fibres, as shown in Equation 2.12. Jones further correlated the delamination growth rate $\frac{da}{dN}$ with the term $(\sqrt{\Delta G}-\sqrt{\Delta G_{th}})$, rather than directly using the expression for Δg, due to the unavailability of comprehensive delamination resistance data, as represented in Equation 2.13.

$$G_{I_C} = G_{\text{tip}} + G_{\text{br}} \tag{2.12}$$

$$\frac{da}{dN} = c_1 \left(\Delta g\right)^{n_1} = c_1 \left(\frac{\sqrt{\Delta G} - \sqrt{\Delta G_{th}}}{\sqrt{1 - \frac{\sqrt{G_{max}}}{\sqrt{A}}}} \right)^{n_1} \tag{2.13}$$

Yao[40] further advanced this concept by applying it to the observations illustrated in Figure 2.8. In this approach, the strain energy release rate (SERR), G_{IC}, was defined using an extended form of the J-integral, originally proposed by Bao[49], as presented in Equation 2.14. In this context, G_b represents the SERR associated with fibre bridging, while l_p^L denotes the length of the process zone, defined as the point at which fully developed fibre bridging occurs.

$$G_R(\Delta a) = \begin{cases} G_{\text{Tip}} + G_b \frac{\Delta a}{l_p^L} & \text{for } \Delta a < l_p^L \\ G_{\text{Tip}} + G_b & \text{for } \Delta a \geq l_p^L \end{cases} \tag{2.14}$$

Using this Yao proposed a modified Paris equation that takes into account the effect of fibre bridging. He adopted the SERR at the tip from a relation proposed by Donough[50] from which he comes up with a modification for the Paris relation as seen in Equation 2.15 where c_2 and n_2 are curve fitting parameters.

$$\frac{da}{dN} = c_2 \left(\Delta G_{eff}\right)^{n_2} = c_2 \left[\frac{G_0}{G_{IC}(a - a_0)} \Delta G \right]^{n_2} \tag{2.15}$$

The proposed modified relation represents a generalized form of the Paris relation, incorporating the effect of fibre bridging, with delamination in the absence of fibre bridging treated as a special case.

Various theoretical models have been developed to characterize fatigue delamination growth in composite materials, many of which incorporate complex models in order to describe the effect of fibre bridging. However, Alderliesten[42] proposed a simplified methodology for calculating a delamination resistance curve that excludes fibre bridging, avoiding the need for theoretical models to describe this phenomenon. His method aligns with his previous proposal that any model for fatigue delamination should relate the crack driving force to the delamination crack growth rate. In his analysis, Alderliesten considered the energy release rate in terms of $\Delta\sqrt{G}$.

Alderliesten's approach requires fatigue test data from a specimen that has undergone multiple test sequences. As previous research has demonstrated, this data can be plotted using the Paris relation, with the G-term represented by $\Delta\sqrt{G}$, as shown in Equation 2.2. In this framework, each data point corresponds to a specific crack length $a - a_0$. Regression is then performed over the surface defined by $\Delta\sqrt{G}$, $a - a_0$, and the crack growth rate da/dN. By linearizing and plotting the data, a surface fit is obtained using the regression equation (Equation 2.16).

$$\log(\Delta\sqrt{G})^2_{reg} = C_0 + C_1(a - a_0) + C_2 \log\left(\frac{da}{dN}\right) + C_3(a - a_0)^2 + C_4 \log\left(\frac{da}{dN}\right)^2 \tag{2.16}$$

In the next step, the term $a - a_0$ is set to zero to calculate $\Delta\sqrt{G}$ using the same regression equation, with the coefficients obtained from the surface fit. This calculated value is then translated to the zero-bridging curve, using the transformation described in Equation 2.17.

$$\log(\Delta\sqrt{G})^2_T = \left[\log(\Delta\sqrt{G})^2 - \log(\Delta\sqrt{G})^2_{reg}\right] + \log(\Delta\sqrt{G})_{a-a_0=0} \tag{2.17}$$

Although this method holds significant potential for generating valid and consistent zero-fibre bridging curves, it remains relatively new and requires further research and validation. One challenge of this approach is that it relies on the availability of multiple test sequences to ensure sufficient fibre bridging development. Without enough data points or sequences, the method becomes inapplicable, limiting its practical use in some scenarios.

2.6. Conclusions from Literature

This chapter provides an overview of key concepts and research relevant to fatigue delamination in composites. It covers the fundamental differences between crack growth in metals and fibre-reinforced polymers (FRPs), focusing on delamination mechanisms under cyclic loading. Various methods for predicting delamination growth, including stress/strain approaches, frac-

ture mechanics, and cohesive zone models, are discussed. Additionally, the chapter explores the effect of fibre bridging on delamination behaviour, the challenges of characterizing it, and the development of predictive models based on strain energy release rate (SERR). These insights are critical to understanding fatigue delamination and informing the standardization of testing methods.

3

Research Objective

Based on the literature study presented in chapter 2, various methodologies for the characterization of delamination growth in fibre-reinforced composites have been analyzed. This review has provided a comprehensive understanding of the critical aspects to consider when analyzing fatigue test data.

A major takeaway from the literature is that Linear Elastic Fracture Mechanics (LEFM) remains the most widely adopted and appropriate framework for defining fatigue delamination growth, particularly in terms of gaining a deeper understanding of the physics underlying key phenomena, including fibre bridging. When attempting to capture the physical processes driving fatigue crack growth, the crack driving force(CDF) emerges as the most suitable parameter for characterizing delamination behaviour. Extensive research, along with SEM analysis, supports the conclusion that the strain energy release rate (SERR) applied directly at the crack tip is the optimal choice for representing this crack driving force.

Another important factor highlighted in the literature is the influence of the stress ratio on delamination growth. While past research largely focused on identifying a single similitude parameter to characterize delamination growth, it has since been recognized that this approach may be insufficient. Because fatigue delamination growth in composites is influenced by both monotonic and cyclic components, a more comprehensive representation is necessary. The correct parameter for composites, analogous to the similitude parameter used in metals, is expressed as $\Delta\sqrt{G} = \left(\sqrt{G_{max}} - \sqrt{G_{min}}\right)^2$. This parameter captures the cyclic load component, while the G_{max} term represents the monotonic load component. A representation between these two and the delamination growth rate in three dimensions will provide a complete picture for the delamination growth rate in composites.

Focusing specifically on the phenomenon of fibre bridging, it is important to note that this effect is predominantly observed during testing on Double Cantilever Beam (DCB) specimens.

Fibre bridging is typically not encountered outside of this specific testing context, which can lead to an underestimation of structural design requirements, as the presence of fibre bridging is known to enhance delamination resistance. The methodologies used to characterize delamination growth have largely been developed through empirical models based on curve fitting of experimental data. However, as highlighted in the literature, there is a general consensus among researchers that a single parameter is insufficient to fully describe delamination growth, given the complexity of the process. As a result, there has been significant research into the development of two-parameter models to account for additional effects such as stress ratio and fibre bridging.

The literature identifies three primary methods for plotting delamination growth data while excluding the influence of fibre bridging:

- Hartman-Schijve Model
- Modified Paris Relation
- Regression Method

Among these, the Modified Paris Relation and the Regression Method are relatively recent approaches, with limited research available on their validation. However, both methods show significant promise based on the current body of studies. Further validation of these methodologies would be a critical first step toward establishing standardized testing procedures for Mode I fatigue delamination in fibre-reinforced polymers.

Therefore, the main objective of this thesis can be summarized as:

> To develop and ISO standard for mode I fatigue delamination testing in fibre reinforced polymer composites

With the main objective established, the next step is to define a set of research questions that will guide the achievement of this objective.

Main Research Question:

> What is the most appropriate method that can be used to ensure convergence to a single delamination growth curve?

Sub-Questions

> SQ1 - What is the optimal parameter for describing similitude in fatigue delamination growth?

SQ2 - What is the most effective methodology for generating a curve that accurately represents fatigue delamination growth without the influence of fibre bridging?

4

Methodology

For this study, the testing was not performed by the author. The test methodology, data reduction, and results discussed and analyzed in this work are derived from existing published data from various sources. The procedures for testing and data reduction outlined in the following sections adhere to three established standards: ASTM E647, ISO 15024, and ASTM D5528.

The ASTM E647 standard titled “Standard Test Method for Measurement of Fatigue Crack growth Rates” is designed to measure the fatigue crack growth rates in materials, expressed in terms of stress intensity factor range ΔK. This standard is essential for understanding the resistance of materials to stable crack growth under cyclic loading which in turn helps in the estimation of the durability and lifespan of the component subjected to this cyclic stress. As previously discussed, using the SIF for characterization, particularly in composites, is not ideal; instead, the SERR should be utilized.

With the use of SERR value for the data reduction of the test data in the case of FRP’s, ISO 15024 and ASTM 5528 recommend methodology for the calculation of the G_{IC} value, where G_{IC} is the SERR for mode I cracks. Three different methods are proposed by both ASTM and ISO for the calculation of the G_{IC} value: Modified Beam Theory (MBT), Compliance Calibration (CC) and Modified Compliance Calibration (MCC). As observed by Yao et al. [51] the difference between the G_{IC} value that is calculated using the 3 different methods differ by no more than 3.1%. Hence for the purpose of this study the MCC method is used for the determination of G_{IC}.

4.1. Test setup and Procedure

According to ASTM E647 guidelines, the DCB specimen must have minimum dimensions of 125 mm by 20 mm, with a minimum thickness of 3 mm for CFRP and 5 mm for GFRP. The dimensions of the specimen was taken to be 200mm by 20mm in order to facilitate the

generation of multiple curves and the thickness was taken to be 5mm to reduce the compliance of the specimen. Two aluminium blocks each measuring 25mm by 20mm was clamped on either side of the specimen in the orientation as indicated in Figure 4.1.

The DCB specimen with fibre orientation 0//0 and 45//45 was manufactured using CFRP M30SC/DT120 prepreg which was arranged in a unidirectional layup of 32 plies with the stacking sequence $[0_{16}//0_{16}]$ and $[(\pm 45/0_{12}/\mp 45)//(\pm 45/0_{12}/\mp 45)]$ respectively. A pre-crack was generated with the help of a 12.7 μm thick Teflon layer during the hand layup process. The composite was then cured in an autoclave based on the cycle prescribed by the manufacturer.

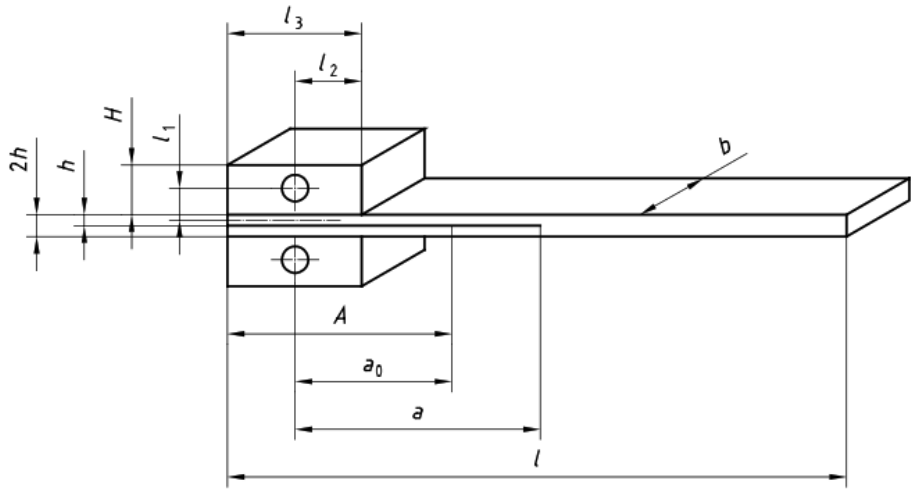

Figure 4.1: Double Cantilever setup with initial delamination

Key

b Specimen width
$2h$ Specimen thickness
a_0 Initial delamination length
a Total delamination length
A Insert length
l Specimen length
l_1 Distance from centre of loading pin (or piano hinge axis) to mid-plane of specimen
l_2 Distance from centre of loading pin (or piano hinge axis) to edge of load block (or piano hinge)
l_3 Block length
H Block thickness

4.1.1. Quasi-Static Delamination Test

The quasi-static delamination test was carried out as recommended by ASTM D5528 where the pre-crack values were determined. A displacement control approach was adopted where the rate of loading was 1mm/min. This quasi-static load is applied until crack propagation is observed. The corresponding displacement value is set as the δ_{max}. Based on the stress ratio

the δ_{min} can be calculated according to Equation 4.1. The same methodology is repeated to determine the pre-crack value for all the subsequent sequences and the cyclic loading in the MTS is programmed to oscillate between these maximum and minimum values.

$$R = \frac{\delta_{min}}{\delta_{max}} \tag{4.1}$$

4.1.2. Fatigue Delamination Growth Tests

Fatigue delamination tests can be conducted using either the force-controlled or displacement-controlled method. The displacement-controlled method is generally preferred, as it facilitates automatic load shedding. As delamination progresses and stiffness decreases, the applied load reduces accordingly, making the process more efficient. In the case of force-control, the specimen compliance increases resulting in larger displacements as the number of cycles increases. The determination of the initial load that can achieve a broad range of crack growth rates is the major drawback of using the force control.

Given this apparent advantage, displacement control is adopted with a frequency of 5Hz. Initially an interval of 100 cycles is taken for the first 5000 fatigue cycles. This was followed by intervals of 500 cycles for the next 15000 cycles. Once the fatigue cycle surpasses 20000 the intervals are increased to every 1000 cycles.

4.2. Data Acquisition and Reduction

The raw data from the testing typically contains the data corresponding to the crack length, force, displacement and cycle number. The data that was published by Yao et al. [51] contained additional data in the form of the delamination growth rate as well as strain energy release rate, but this was not taken into consideration as it was not a part of ideal raw data and is thus excluded from the analysis.

4.2.1. Delamination Growth Rate Calculation

The delamination growth rate can be calculated using an incremental polynomial method. The ASTM E647 standard prescribes the use of either the secant method or the 7 point polynomial method for the calculation of the delamination growth rate as illustrated in Figure 4.2.

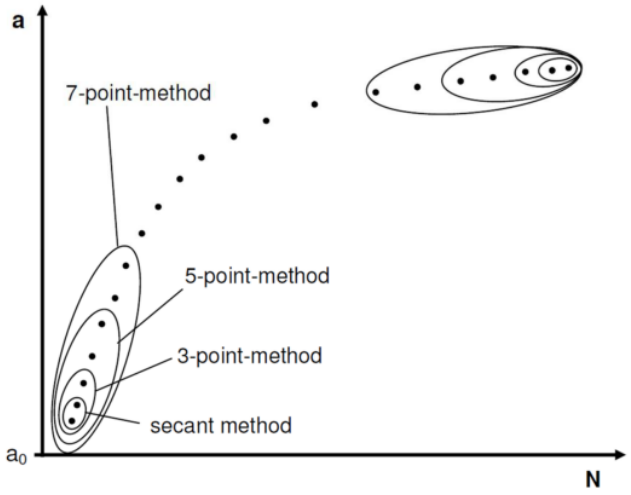

Figure 4.2: Schematic representation of incremental polynomial method

In the secant method the value can be determined by the calculation of the slope between 2 adjacent data points in a plot between the crack length and the number of cycles as indicated by Equation 4.2.

$$\frac{da}{dN} = \frac{(a_{i+1} - a_i)}{(N_{i+1} - N_i)} \tag{4.2}$$

The 7-point incremental method is used in this analysis and is more complex compared to the secant method. A second order polynomial is fitted to sets of 2n + 1 successive data points where n = 3. The equation of the polynomial fit is:

$$\hat{a}_i = b_0 + b_1 \left(\frac{N_i - C_1}{C_2} \right) + b_2 \left(\frac{N_i - C_1}{C_2} \right)^2 \tag{4.3}$$

where:

$$-1 \leq \left(\frac{N_i - C_1}{C_2} \right) \leq +1 \tag{4.4}$$

The parameters b_0, b_1, and b_2 are regression coefficients determined by the least squares method over the range $a_{i-n} \leq a \leq a_{i+n}$. To avoid numerical difficulties in calculating the regression parameters, the following values for C_1 and C_2 are used to scale the input parameters:

$$C_1 = \frac{1}{2}(N_{i-n} + N_{i+n}) \tag{4.5}$$

$$C_2 = \frac{1}{2}(N_{i+n} - N_{i-n}) \tag{4.6}$$

4.2.2. Strain Energy Release Rate Calculation

As outlined at the beginning of this chapter, due to the minimal variation in the SERR values calculated using the modified beam theory, compliance calibration, and modified compliance calibration methods, the Modified Compliance Calibration method is recommended for use in this thesis.

The first step in the calculation of the strain energy release rate using MCC is the calculation of the compliance value. Equation 4.7 can be used for this purpose where the D represents the displacement and P represents the force. This is followed by a plot between $C^1/3$ and a/h, where the slope of this plot gives the value of A_1.

$$C = \frac{(D_{max} - D_{min})}{(P_{max} - P_{min})} \tag{4.7}$$

Using the calculated values the G_{IC} can be calculated using Equation 4.8, where C is the compliance, B is the width of the specimen and h is the thickness of the specimen. G_{max} and G_{min} can be calculated by using P_{max} and P_{min} respectively.

$$G_I = \frac{3P^2C^{(2/3)}}{2A_1Bh} \tag{4.8}$$

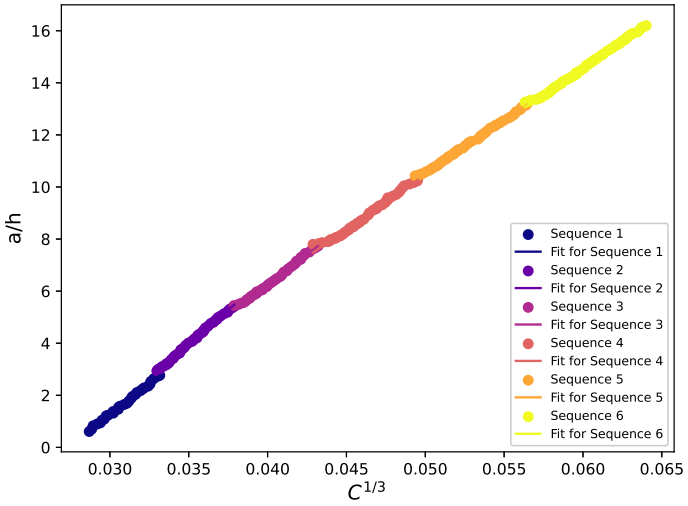

Figure 4.3: $C^{1/3}$ vs a/h for Specimen 7

4.3. Reduction Methods

Since two different methodologies are implemented in this thesis, the approach for each is detailed in the following sub-sections. The challenges encountered during implementation, along with a comparison of the different approaches that could be applied, are discussed in the subsequent chapter.

4.3.1. Regression Method

From previous discussions it is clear that there is no consensus on the choice of the parameter that can be used as a similitude. For this purpose, two of the most prominent choices: $\Delta(\sqrt{G})$ and G_{max} are used to plot the data and analysis is done on the basis of the results. The selection of these two parameters is based on findings from the literature, highlighting their dependence on both cyclic and monotonic load components.

Paris relation has been used for the characterization of the crack growth rate where the da/dN values are plotted against the similitude parameter which in this case is either $\Delta(\sqrt{G})$ or G_{max} following the relations:

$$\frac{da}{dN} = C(\Delta\sqrt{G})^n \tag{4.9}$$

$$\frac{da}{dN} = C^{'}(G_{max})^{n^{'}} \tag{4.10}$$

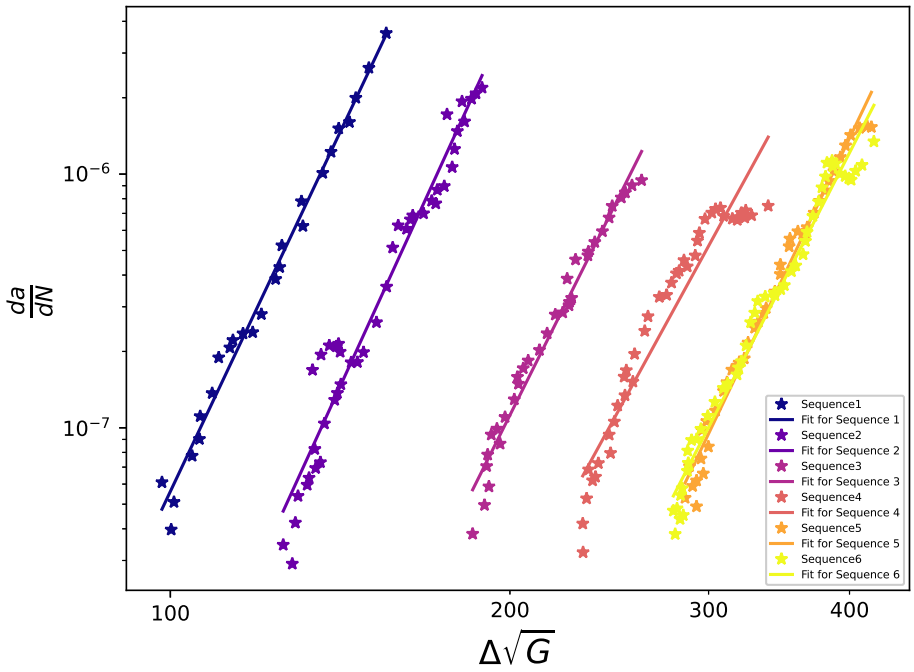

Figure 4.4: Paris Curve Representation of Fatigue Delamination Growth with $\Delta\sqrt{G}$ for Specimen 7

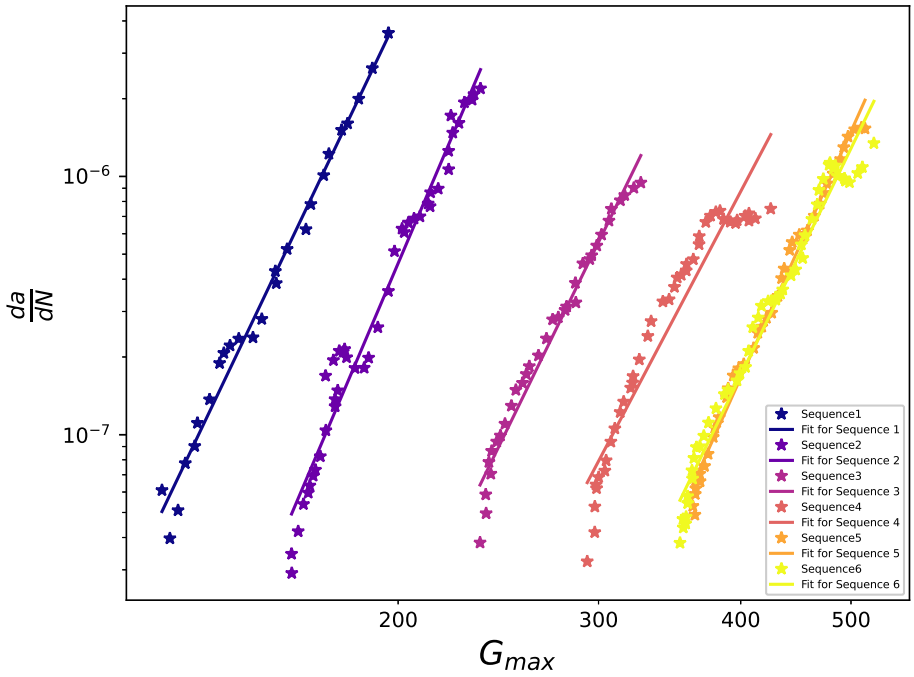

Figure 4.5: Paris Curve Representation of Fatigue Delamination Growth with G_{max} for Specimen 7

Alderliesten[42] proposed the regression equation where the value of $(\Delta\sqrt{G})^2_{reg}$ is plotted as a function of the crack length and the crack growth rate as shown in Equation 4.11. Here, the C_0, C_1, C_2, C_3 and C_4 are the constants that are obtained from the regression fit.

$$log(\Delta\sqrt{G})^2_{reg} = C_0 + C_1(a - a_0) + C_2 log(\frac{da}{dN}) + C_3(a - a_0)^2 + C_4 log(\frac{da}{dN})^2 \tag{4.11}$$

A zero-bridging curve can be generated from this regression by setting the value of $a - a_0$ equal to zero and then plotting the curve. It must be noted that the coefficients in the zero-bridging equation is taken from the initial regression fit. Equation 4.12 shows the zero bridging relation.

$$log(\Delta\sqrt{G})^2_{reg} = C_0 + C_2 log(\frac{da}{dN}) + C_4 log(\frac{da}{dN})^2 \tag{4.12}$$

All the generated data and the scatter can be translated to obtain the zero bridging curve using Equation 4.13.

$$log(\Delta\sqrt{G})^2_T = [log(\Delta\sqrt{G})^2 - log(\Delta\sqrt{G})^2_{reg}] + log(\Delta\sqrt{G})_{a-a_0=0} \tag{4.13}$$

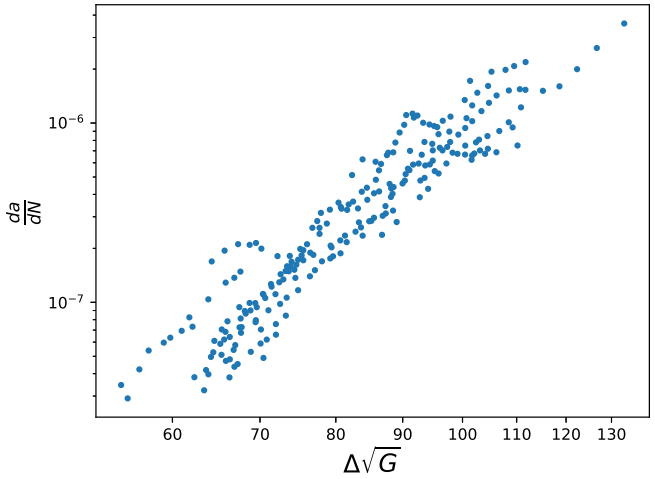

Figure 4.6: Zero Bridging using Regression Method for Specimen 7

4.3.2. Modified Paris Relation

The second method that is implemented is the modified Paris relation that was proposed by Yao et al. [40]. He hypothesized that the SERR that is directly applied on the crack is a better choice for the crack driving force and the representation of the power law relation based on this can be used to represent fatigue delamination growth behaviour.

The method was proposed based on the idea that was proposed by Donough et al. [50] where he proposed a proportional relation for G_{tip} which correlated to the applied SERR in the loading and unloading cycle as shown by Figure 4.7. The proposed relation was as follows:

$$G_{tip} = \frac{G_{max}^{tip}}{G_{max}^{app}} G_{app} \tag{4.14}$$

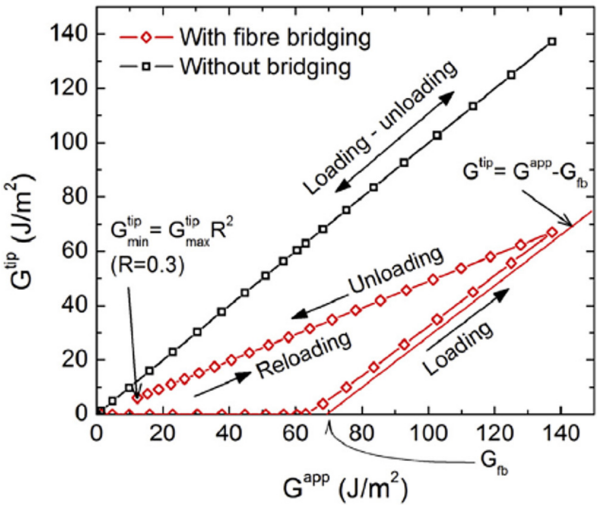

Figure 4.7: G_{tip} in fatigue when fibre bridging is present[50]

From this relation the G_{max}^{app} is comparable to $G_{IC}(a - a_0)$ for the case where the maximum load at the end of the loading phase is equal to the critical load. This results in the following relation for G_{tip}:

$$G_{tip} = \frac{G_0}{G_{IC}(a - a_0)} G_{app} \tag{4.15}$$

The G_0 in Equation 4.15 is equal to G_{max}^{tip} which represents the initial delamination resistance. For the determination of the G_{IC} the R-curve needs to be created. This method is implemented to enable a comparison with the regression method. Consequently, an effort was made to replicate the results obtained by Yao et al. [40] to the greatest extent possible. The function for G_{IC} is obtained from this R-curve plot which can be generated by plotting the G_{max} calculated by the MCC method against the corresponding $a - a_0$ value as seen in Figure 4.8a. Using Equation 4.16 the modified Paris relation with fibre bridging can be plotted.

$$\frac{da}{dN} = c\,(\Delta G_{eff})^n = c\left[\frac{G_0}{G_{IC}(a - a_0)} \Delta G\right]^n \tag{4.16}$$

The c and n in the equation similar to the other cases act as curve fits for the proposed relation. An important note needs to be taken for the fact that the mentioned relation is the general form of the Paris relation with fibre bridging and the fatigue delamination without fibre bridging is just a special case of this relation.

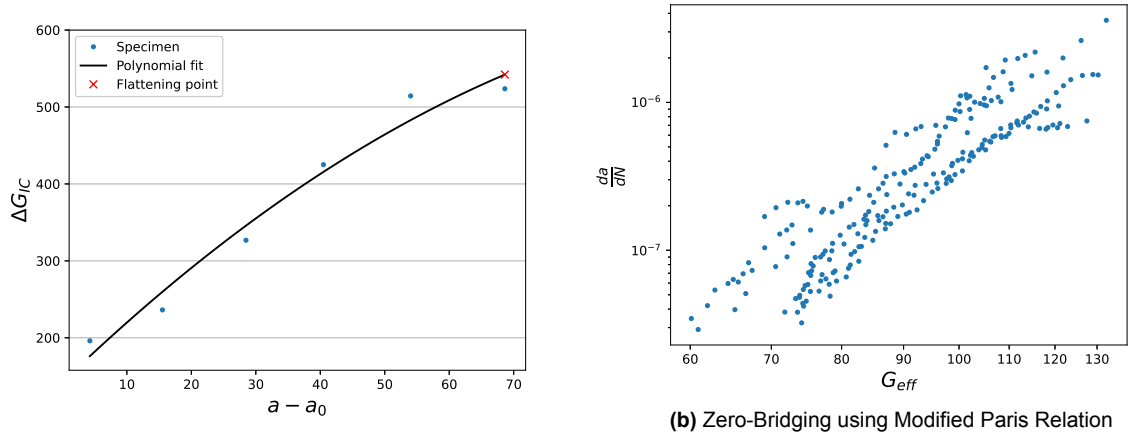

(a) R-curve for Specimen 7

(b) Zero-Bridging using Modified Paris Relation for Specimen 7

Figure 4.8: Modified Paris Relation Implementation

4.4. Validation Methods

Two primary validation methods have been employed in this thesis to ensure both the proper implementation of the methodology and the assessment of data scatter. The first validation method focuses on verifying the accuracy of the implementation. This is achieved by reverse-

implementing the methodology to determine if the predicted curves lie within the 95% confidence interval, thereby confirming the reliability of the model in capturing the expected range of outcomes.

The second validation method utilizes the cumulative distribution function (CDF) to evaluate the quality of data scatter and the goodness of fit. This approach provides a comprehensive assessment of how well the data distribution is represented across different implementations of the same dataset, particularly when data sizes vary. Analyzing the degree of scatter and the quality of the fit offers a comprehensive assessment of the proposed method's performance. Together, these validation methods provide a rigorous framework for evaluating both the fidelity of the implementation and the statistical soundness of the data analysis.

4.4.1. Translated Curve Implementation Check

To verify the robustness of the translated curve implementation, an approach opposite to the initial methodology was applied. In this approach, two boundary data points were selected from each dataset within the translated curve. These points represent key positions on the curve, capturing the extremes of the data distribution. For each boundary point, the pre-crack length associated with a specific crack growth rate, denoted as da/dN, was added to the translated $\Delta\sqrt{G}$ value. This cumulative value was then used to construct a predicted curve for each sequence, intended to represent the modified behaviour of the material under a controlled translation of the fracture energy values.

Following this, the original sequence data was plotted as the baseline experimental data. Alongside this experimental data, a 95% confidence interval was established to define the range of expected values based on the original dataset. The predicted translated data was then plotted and assessed for whether it fell within this confidence interval. By evaluating the translated curves in relation to this interval, it was possible to determine if the predictive implementation maintained the expected statistical distribution and was consistent with observed behaviour.

Although this methodology may not be ideal for accurate future predictions due to its assumption of linearity and reliance on specific boundary points, it provides a strong basis for verification. The key challenge addressed here is the slope disparity between the translated and experimental data curves. The translated curve often exhibits a steeper slope than the experimental data, which, if left uncorrected, would imply a mismatch in the rate of crack growth across different crack lengths.

A simple translation of data points based solely on pre-crack length would result in a predicted curve with a similar slope to the original zero-bridging data, failing to capture the necessary changes in behaviour. By accounting for the adjusted slope, this methodology corrects for such discrepancies, allowing the predicted curve to more accurately reflect the experimental trend. As a verification step, this approach ensures that the translation process is effectively implemented, yielding a curve with an appropriate slope that more closely aligns with observed

behaviour, thus enhancing the validity of the method in capturing progressive damage characteristics in the material.

4.4.2. Cumulative Distribution Function

The methodology for developing a Cumulative Distribution Function (CDF) serves as an essential data quality assurance step, allowing for the systematic evaluation of data scatter and the subsequent analysis of the influence of sample size on the quality of the fit obtained. This step is particularly crucial within the context of this thesis, where a comprehensive understanding of crack growth behaviour and its variability is needed for the accurate comparison between the different implementations.

To implement the CDF, the data points are first translated to a specific level of crack growth rate, denoted as da/dN, and then ranked in ascending order from the lowest to the highest value. Once the data points are ranked, a probability is assigned to each data point using the formula:

$$P = \frac{n}{n_{\text{total}} + 1}$$

where n is the rank number of the data point, and n_{total} represents the total number of data points for that particular curve. This method ensures that each data point is appropriately weighted in terms of its contribution to the overall distribution, enabling a meaningful assessment of data scatter.

The assignment of probabilities allows for a clearer understanding of the distribution characteristics, particularly when comparing datasets of varying sizes. This method allows for assessing and gaining a deeper understanding of the impact of data size on the model fit. Moreover, the cumulative distribution can be graphically represented to visualize the distribution trends and to detect any anomalies or outliers that may indicate data quality issues. This graphical representation also aids in comparing multiple datasets, providing a visual means of assessing whether the scatter in the data is consistent across different sample sizes or experimental conditions.

Additionally, this approach can be extended to incorporate various statistical metrics, such as confidence intervals or goodness-of-fit tests, to further validate the accuracy and consistency of the model. By rigorously assessing the data scatter, the analysis ensures that any conclusions drawn from the models are well-founded and robust against the inherent variability in the experimental data.

5

Results and Discussion

The data analyzed in this study was used to compare different stress ratios and interface conditions. As previously mentioned, the experimental tests were not performed as part of this research; instead, the data was obtained from a previously published study. Table 5.1 presents the details of the stress ratios and interface conditions that were considered for the analysis.

Specimen	Interface	Stress Ratio
Specimen 7	0//0	0.1
Specimen 11	0//0	0.1
Specimen 10	0//0	0.5
Specimen 12	0//0	0.5
Specimen 33	45//45	0.1
Specimen 34	45//45	0.5
Specimen 41	45//45	0.7
Specimen 47	+45//-45	0.5
Specimen 53	+45//-45	0.1
Specimen 54	0//0	0.5
Specimen 55	0//0	0.5
Specimen 56	0//0	0.5

Table 5.1: Summary of Specimen Data used for Analysis

The data in Table 5.1 was originally used by Yao in his thesis, where he proposed a modified

Paris relation and performed detailed analyses on Specimen 7 and Specimen 11. Furthermore, Specimens 10, 12, and 54 were used by Yao in a subsequent validation study. According to the principle of similitude, specimens with the same interface, stress ratio, and material properties are expected to exhibit similar crack growth behaviour. Therefore, specimens with identical interface and stress ratio conditions are compared in this study.

5.1. Zero Bridging using Regression

The concept of similitude implies that specimens with the same interface orientation, stress ratio, and $\Delta\sqrt{G}$ will exhibit identical crack growth rates, da/dN, across different specimens. This assumption relies on $\Delta\sqrt{G}$ as the primary similitude parameter governing crack growth.

The choice of an appropriate method must be closely aligned with the selection of the similitude parameter, as both decisions are interdependent. For the proposed model to be effective, selecting the correct similitude parameter is crucial. With this approach, the methodology proposed by Alderliesten[42] was evaluated using both $\Delta\sqrt{G}$ and G_{max} as potential similitude parameters. While literature suggests that two parameters are generally required—one representing the monotonic load component and the other the cyclic load component—individual analyses of each parameter were conducted to understand the trends they exhibit. This analysis specifically focused on Specimens 7 and 11, as prior studies have also examined these specimens helping establish a baseline to validate the correct implementation of the methodology.

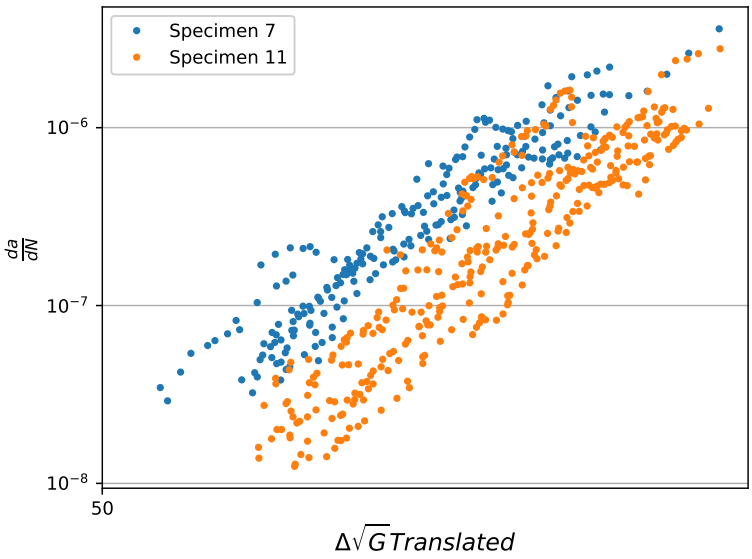

Figure 5.1: Regression-Based Zero-Bridging Curve for Specimens 7 and 11(R=0.1) Using $\Delta\sqrt{G}$

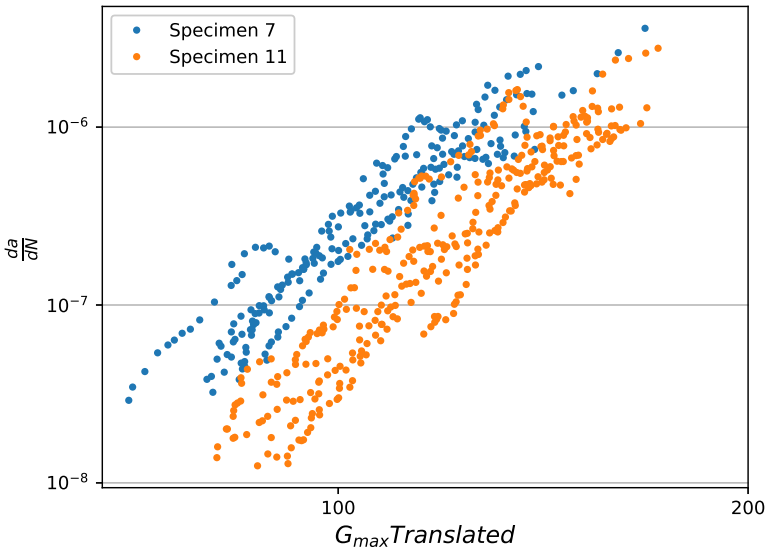

Figure 5.2: Regression-Based Zero-Bridging Curve for Specimens 7 and 11(R=0.1) Using G_{max}

The plots in Figure 5.1 and Figure 5.2 reveal a clear correlation between the zero-bridging curves for both specimens, even though they do not align perfectly. Notably, when G_{max} is used in the regression analysis, the curve for Specimen 11 shows a slight deviation from that of Specimen 7 along the x-axis. For comparison, the zero-bridging curves for Specimens 10 and 12, tested with a stress ratio of 0.5, are also presented.

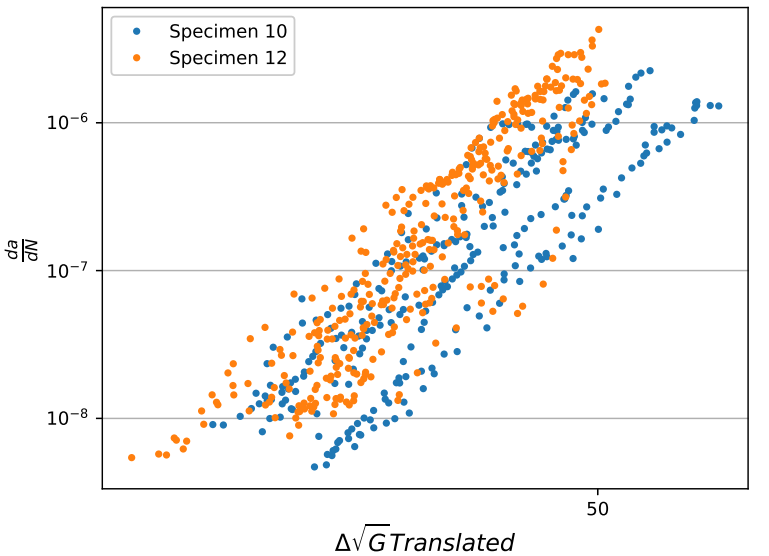

Figure 5.3: Regression-Based Zero-Bridging Curve for Specimens 10 and 12(R=0.5) Using $\Delta\sqrt{G}$

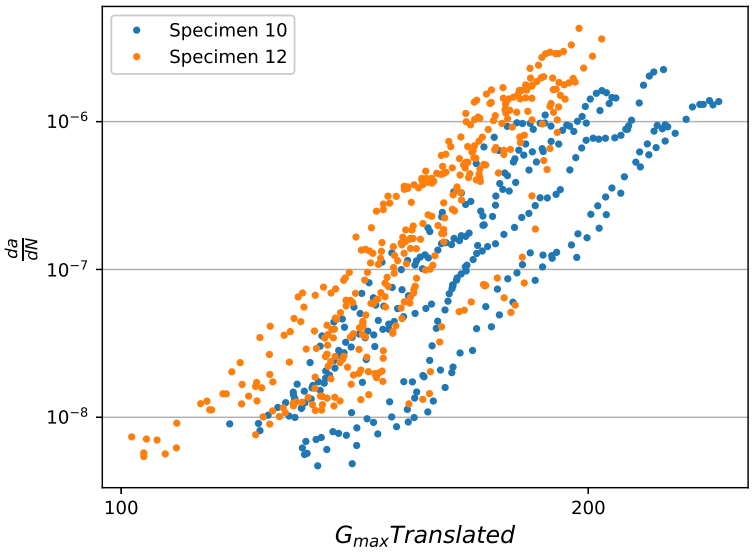

Figure 5.4: Regression-Based Zero-Bridging Curve for Specimens 10 and 12(R=0.5) Using G_{max}

A noticeable difference in correlation is observed between the two curves when comparing specimens with a stress ratio of 0.5 to those with a stress ratio of 0.1. This variation in correlation also depends on the choice of parameter, whether $\Delta\sqrt{G}$ or G_{max} is used. To substantiate this observation, a cumulative distribution function (CDF) comparison between the two parameters would provide deeper insights into the level of correlation across the datasets represented by the curves.

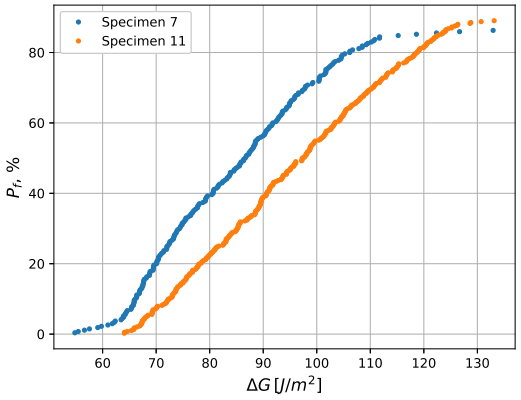

(a) Cumulative Probability Distribution Function using $\Delta\sqrt{G}$

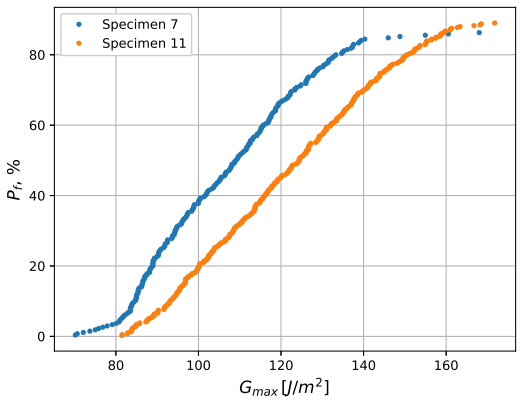

(b) Cumulative Probability Distribution Function using G_{max}

Figure 5.5: Comparison of Correlation using CDF for different similitude parameters R=0.1

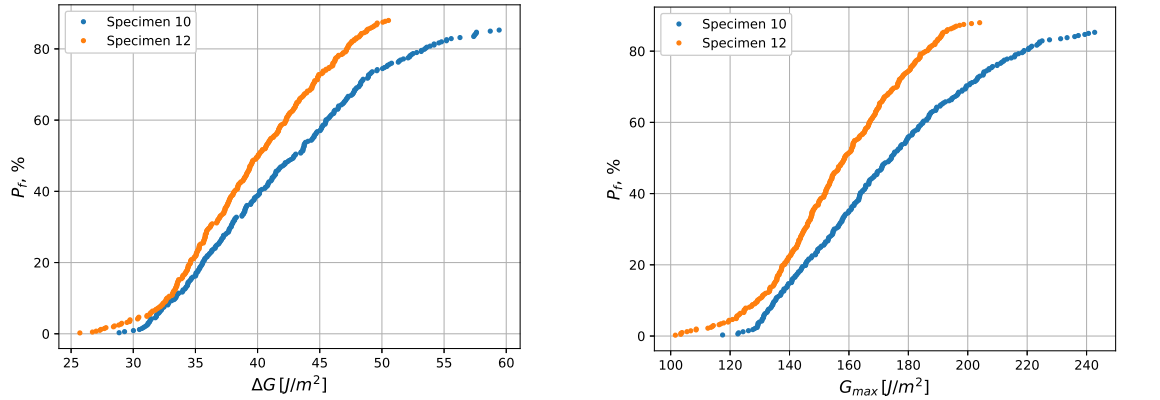

(a) Cumulative Probability Distribution Function using $\Delta\sqrt{G}$ **(b)** Cumulative Probability Distribution Function using G_{max}

Figure 5.6: Comparison of Correlation using CDF for different similitude parameters R=0.5

Literature findings highlight the importance of considering both monotonic and cyclic load components to accurately characterize fatigue delamination growth rates and achieve a thorough understanding of the process. Most prior studies have attempted to integrate these two components within a single equation to capture the interdependence between the parameters effectively.

Both the Hartman-Schijve and Modified Paris Relation share an intriguing commonality in their approach to characterize fatigue delamination growth. Both of the proposed equations use two key parameters to characterize the crack growth rate: $\Delta\sqrt{G}$ and G_{max}. A critical feature of both equations is the denominator term, which acts as a delamination resistance factor. In the Modified Paris relation, the $G_{IC}(a - a_0)$ term effectively captures the variation in G_{max} as a function of $a - a_0$.

$$\frac{da}{dN} = c_1 \left(\Delta g\right)^{n_1} = c_1 \left(\frac{\sqrt{\Delta G} - \sqrt{\Delta G_{th}}}{\sqrt{1 - \frac{\sqrt{G_{max}}}{\sqrt{A}}}} \right)^{n_1} \tag{5.1}$$

$$\frac{da}{dN} = c_2 \left(\Delta G_{eff}\right)^{n_2} = c_2 \left[\frac{G_0}{G_{IC}(a - a_0)} \Delta G \right]^{n_2} \tag{5.2}$$

Yao et al. et al. [40] compared the Modified Paris relation he proposed with the Hartman-Schijve model, demonstrating better performance of the Modified Paris relation. Consequently, this study focuses on comparing the regression method with the Modified Paris relation. However, due to differing interpretations regarding the implementation methodology for the Modified Paris relation, as discussed in detail in section 5.3, both implementations are presented for clarity in Figure 5.7 to facilitate discussion.

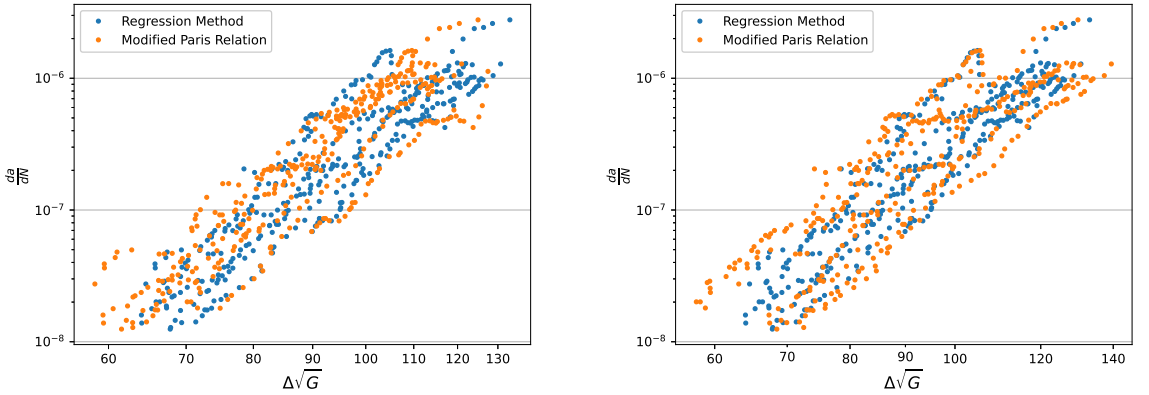

(a) Modified Paris Relation using Bi-Linear Fit from Paper for Specimen 11

(b) Modified Paris Relation using Individual Polynomial Fit from Paper for Specimen 11

Figure 5.7: Comparison of Regression and Various Implementations of the Modified Paris Relation for Specimen 11

This difference in the interpretation of the methodology arises from the calculation of the G_{eff} term. Despite the differences in implementation, the two curves exhibit significant overlap. Notably, this correlation, especially in the case of the regression method, was achieved by using only $\Delta\sqrt{G}$ as the sole similitude parameter. In light of the initial hypothesis, attempts were made to include G_{max} as either a separate term or a cross term in the existing regression equation. Early iterations of these attempts resulted in the regression equation appearing as shown in Equation 5.3 where, a sixth coefficient was introduced, which was related to the G_{max} term.

$$\log(\Delta\sqrt{G})^2_{\text{reg}} = C_0 + C_1(a-a_0) + C_2\log\left(\frac{da}{dN}\right) + C_3(a-a_0)^2 + C_4\log\left(\frac{da}{dN}\right)^2 + C_5\log(G_{max}) \tag{5.3}$$

The resulting regression curve, shown in blue in Figure 5.8, exhibits significant scatter. Given the initial correlation between the Modified Paris Relation and the regression curves, the Modified Relation curve is considered the baseline for comparison. Various iterations of the regression equation were tested, incorporating the G_{max} term either independently or as part of cross terms. However, most of these iterations yielded inconclusive results, with the plot either resembling the one in Figure 5.8 or, in some cases, matching Figure 5.7, though in the latter, the coefficients related to the G_{max} term were effectively zero. This led to the conclusion that this methodology is not the most suitable approach for incorporating the G_{max} term.

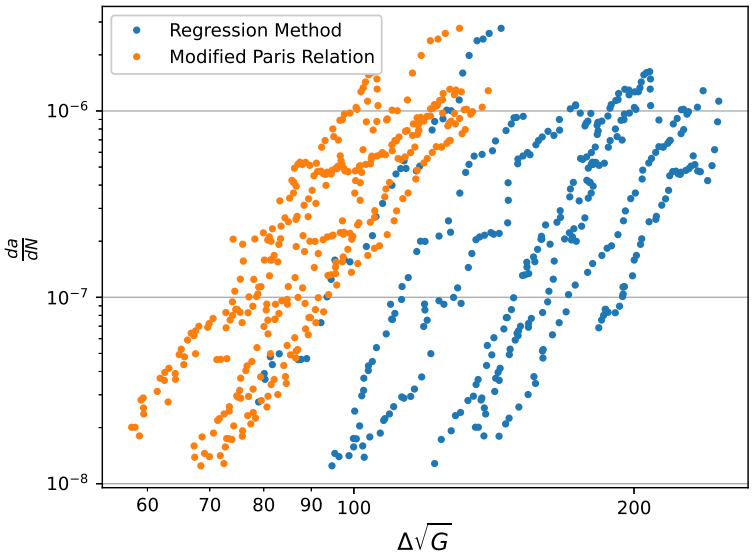

Figure 5.8: Regression Method with an additional term for G_{max}

To refine the approach and better understand the role of G_{max} in the regression equation, it is crucial to consider the effect of the stress ratio. In Yao's validation study[32] of the Modified Paris relation, the effect of the stress ratio was analyzed and presented, as shown in Figure 5.9.

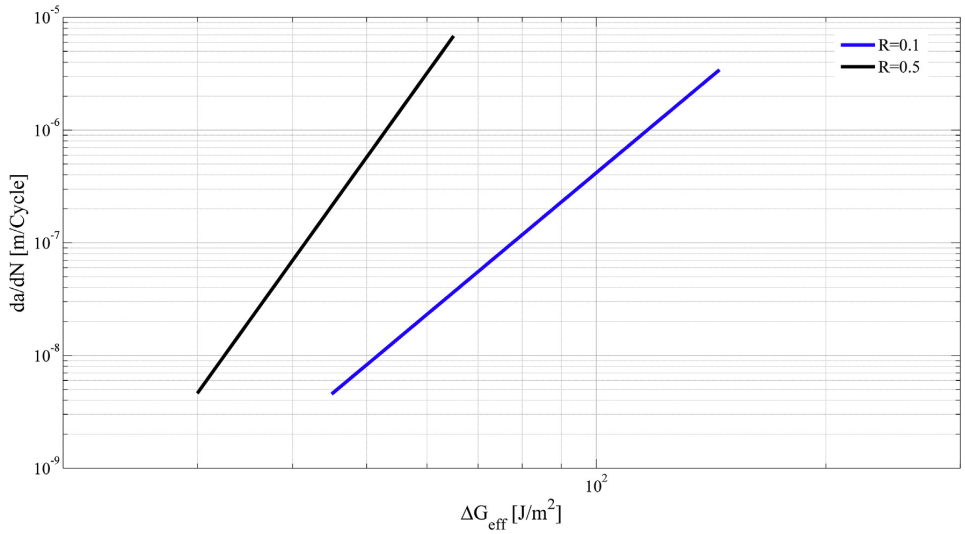

Figure 5.9: Effect of Stress Ratio when using the Modified Paris Relation[32]

Based on this, it is reasonable to expect a similar trend when plotting the zero-bridging curve using the regression method. Indeed, when the plot is generated, as seen in Figure 5.10, a comparable behaviour is observed. However, a more intriguing result emerges when the data is plotted against G_{max}, as previously done. As shown in Figure 5.11, an opposite trend is noted. Further analysis of specimens with different stress ratios revealed a consistent trend across all cases.

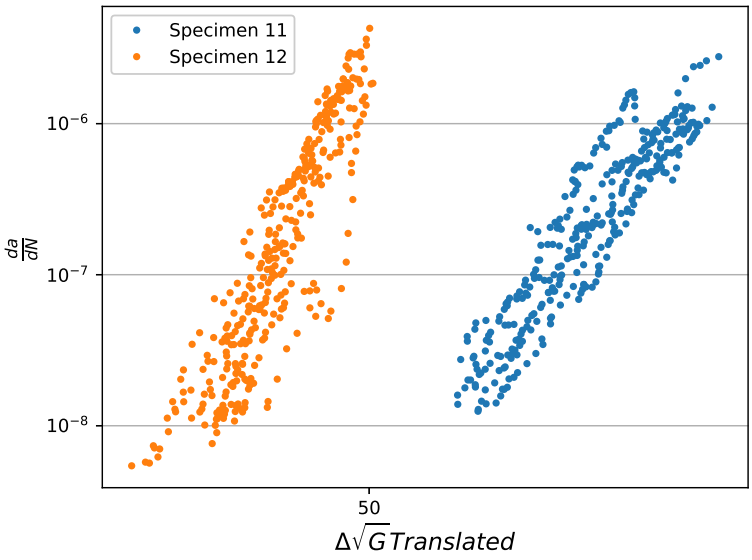

Figure 5.10: Comparison of Regression Method Using $\Delta\sqrt{G}$ for Stress Ratios 0.1 and 0.5

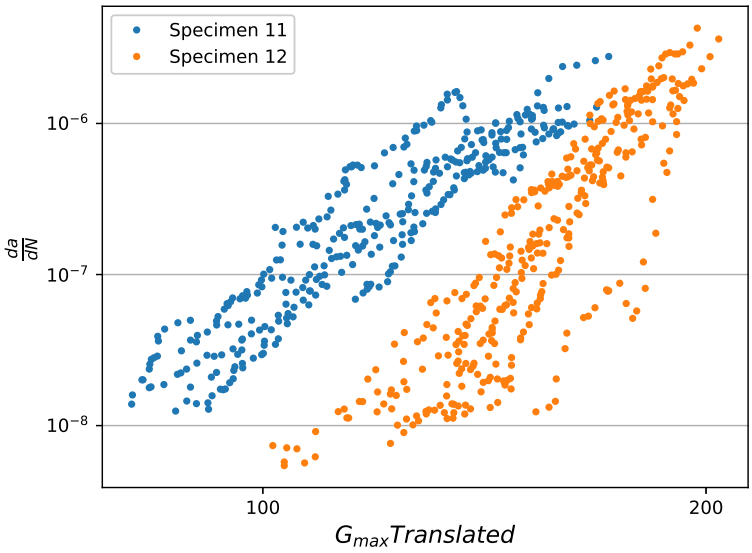

Figure 5.11: Comparison of Regression Method Using G_{max} for Stress Ratios 0.1 and 0.5

This variation in behaviour indicates that a 3D plot could better illustrate the correlation between the three parameters. Plotting the data from the two specimens in terms of translated $\Delta\sqrt{G}$, G_{max}, and da/dN reveals, as shown in Figure 5.12, that the data points for specimens with the same stress ratio align within a single plane.

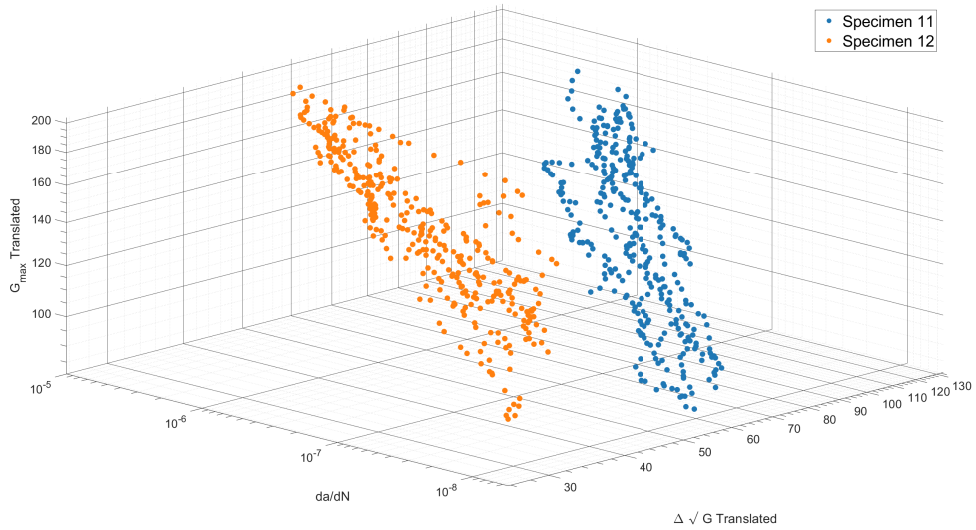

(a) 3D plot between $\Delta\sqrt{G}$, G_{max} and da/dN

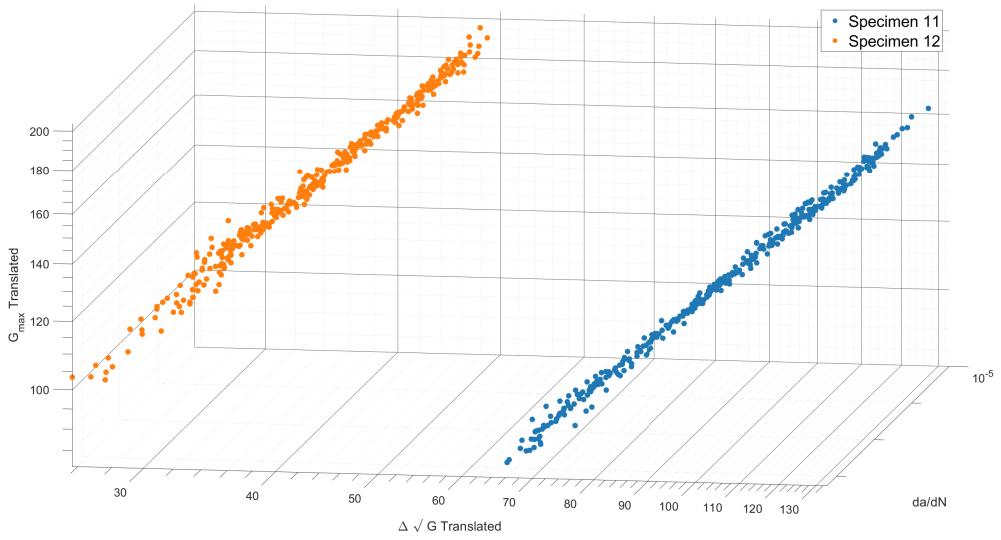

(b) 3D plot between $\Delta\sqrt{G}$, G_{max} and da/dN

Figure 5.12: Combined 3D Plots of $\Delta\sqrt{G}$, G_{max}, and da/dN for Stress Ratios 0.1 and 0.5

The plots in Figure 5.12 demonstrate a clear pattern when the zero-bridging curves are plotted in the three-dimensional space, relating the translated values of G_{max} and $\Delta\sqrt{G}$ against da/dN. This behaviour is further validated by analyzing the data from Specimen 33, Specimen 34, and Specimen 41. As shown in Table 5.2, these specimens share the same interface but differ in their applied stress ratios, with values of 0.1, 0.5, and 0.7, respectively where a separate plane is obtained for each of the different stress ratios.

When plotting specimens with the same stress ratio, it is observed that their data points lie on the same plane, as shown in Figure 5.13, where the translated data for specimens 7 and 11 are presented in 3D. This in comparison to the plot shown in Figure 5.14 and Figure 5.12

demonstrates that the stress ratio is the key factor distinguishing the plane location for the data points. Notably, Specimen 41, which has a higher stress ratio, shows significantly more scatter in the translated zero-bridging curve compared to the other two specimens, where scatter decreases as the stress ratio is reduced. This behaviour suggests a possible relationship between the stress ratio and the scatter in the translated data. However, this relationship could not be confirmed due to insufficient data, particularly for specimens with higher stress ratios.

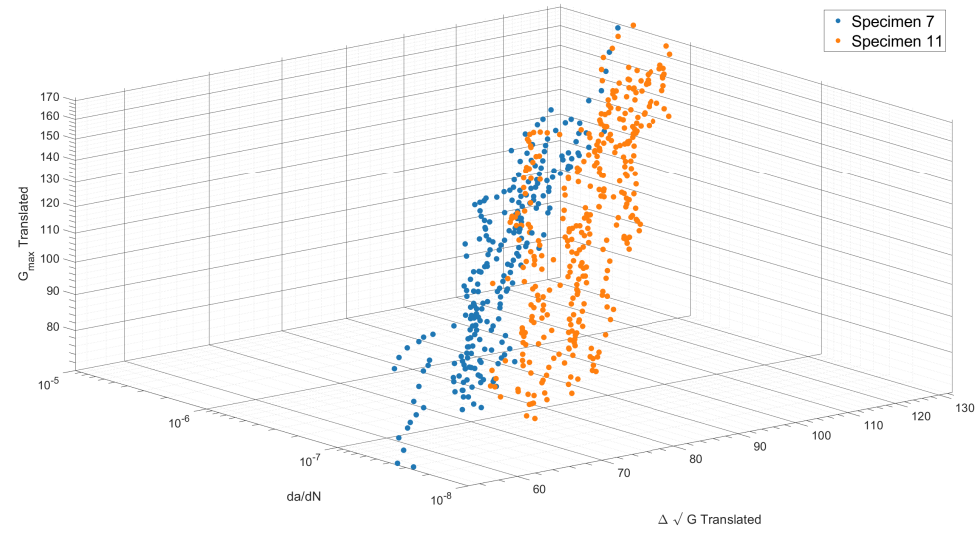

(a) 3D plot between $\Delta\sqrt{G}$, G_{max} and da/dN

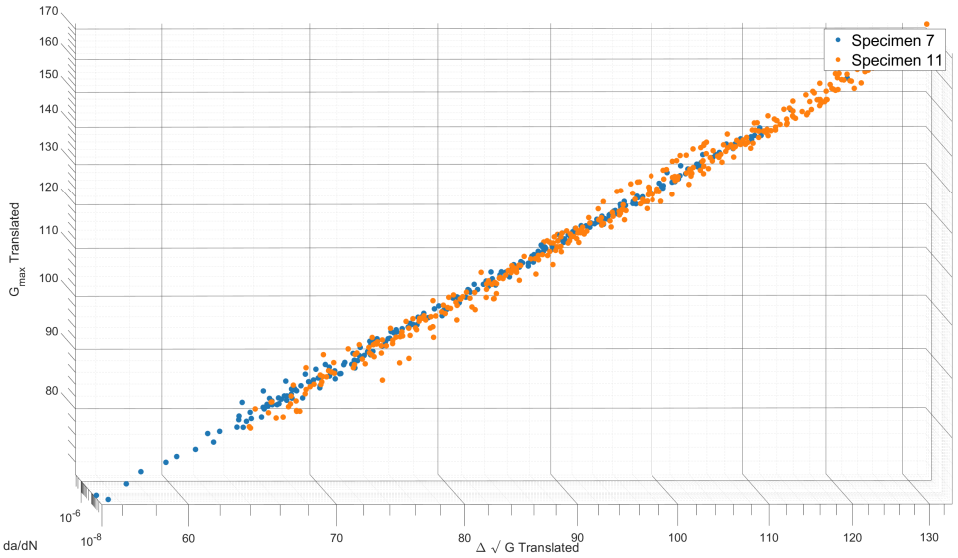

(b) 3D plot between $\Delta\sqrt{G}$, G_{max} and da/dN

Figure 5.13: Combined 3D Plots of $\Delta\sqrt{G}$, G_{max}, and da/dN for Stress Ratio 0.1

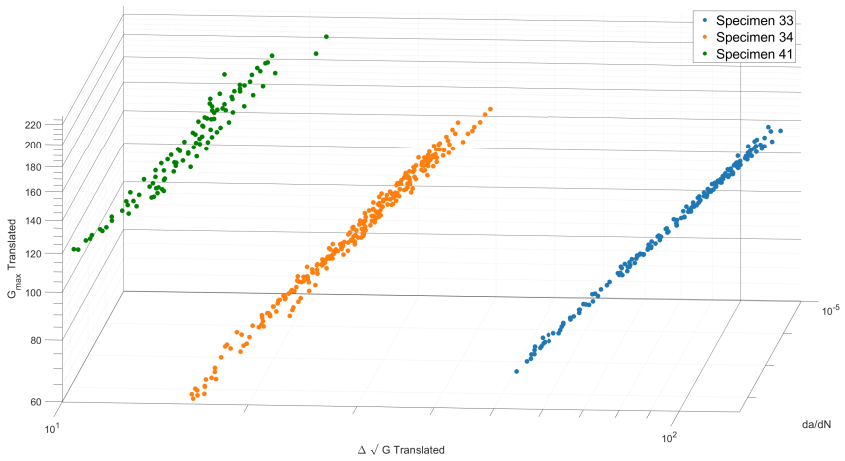

Figure 5.14: Combined 3D Plots of $\Delta\sqrt{G}$, G_{max}, and da/dN for Specimens 33 ($R = 0.1$), 34 ($R = 0.5$), and 41 ($R = 0.7$)

5.1.1. Varying Orientations

In the previous section, the generated 3D plots demonstrated that, for specimens with identical stress ratios, the zero-bridging curves produced through regression analysis lie on the same plane. When the stress ratio is altered, however, the data points shift to distinct planes, indicating a clear dependence of the zero-bridging plane orientation on the stress ratio. This raises the question of how the plot behaviour might change when different fibre orientations are plotted within the same 3D space, while maintaining a consistent stress ratio across all orientations.

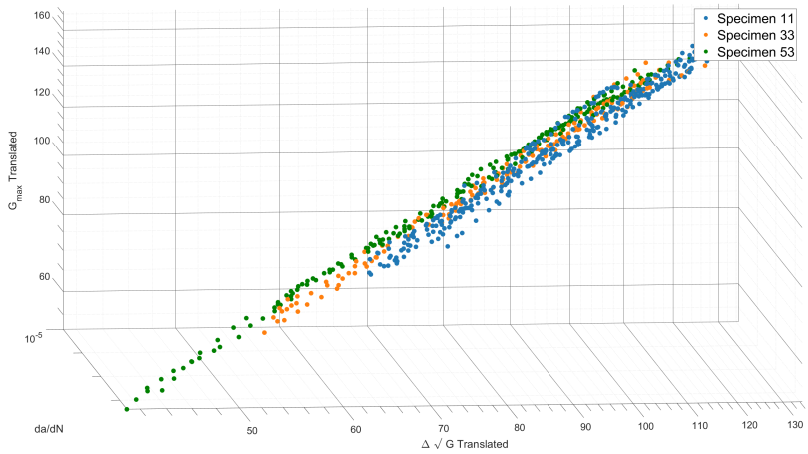

(a) Combined 3D plot for the same stress ratio $R = 0.1$ and varying orientations

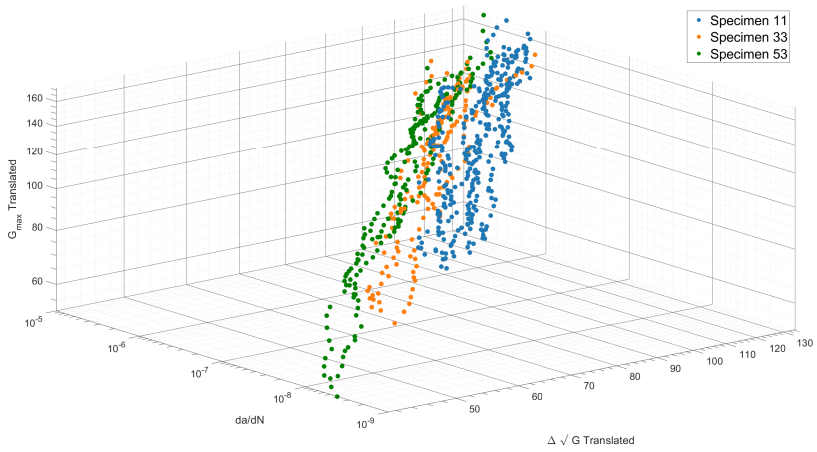

(b) Combined 3D plot for the same stress ratio $R = 0.1$ and varying orientations

Figure 5.15: Comparison of 3D plots for the same stress ratio $R = 0.1$

By examining data for various interface orientations—namely, the 0//0, 45//45, and 45//-45 configurations—and plotting the crack growth rate (da/dN), energy release rate increment ($\Delta\sqrt{G}$), and maximum energy release rate (G_{max}) in 3D space, further insights into orientation effects on the zero-bridging behaviour are obtained.

The primary observation from these 3D plots is that, irrespective of orientation differences, the zero-bridging curves consistently lie on the same plane as long as the stress ratio remains constant. This reinforces the concept that the stress ratio is the primary driver for positioning the zero-bridging plane within the 3D plot. An interesting pattern emerges when comparing the zero-bridging curves of different orientations but identical stress ratios: the 45//45 and 45//-45 interface curves are closely aligned with each other, while the curve for the 0//0 interface is more distant from these two, showing a distinct separation.

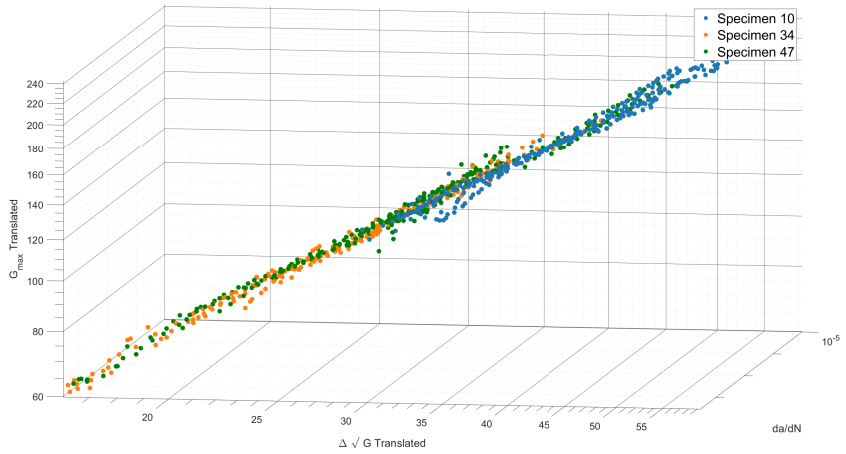

(a) Combined 3D plot for the same stress ratio $R = 0.5$ and varying orientations

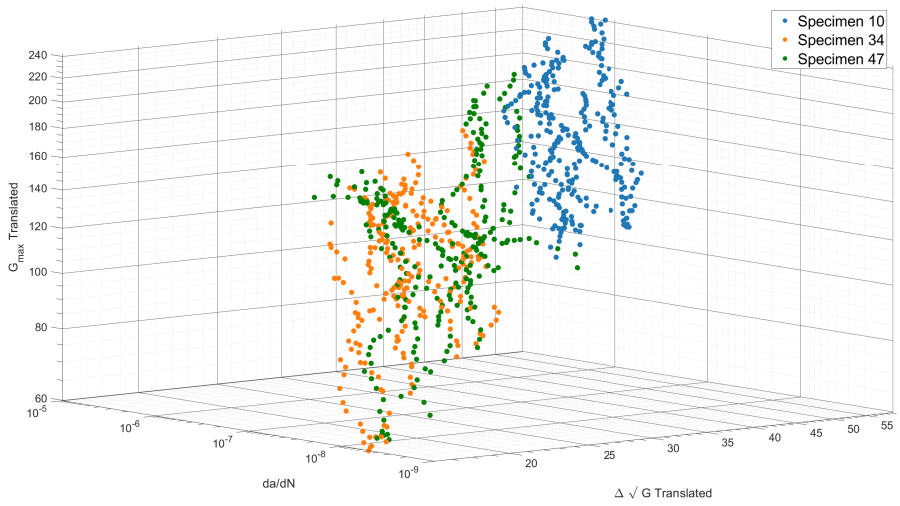

(b) Combined 3D plot for the same stress ratio $R = 0.5$ and varying orientations

Figure 5.16: Comparison of 3D plots for the same stress ratio $R = 0.5$

This behaviour holds true for both stress ratios examined, 0.1 and 0.5, indicating a robust trend across different loading conditions. These observations suggest that, while the stress ratio dictates the plane in which the zero-bridging data lies, the fibre orientation influences the proximity and grouping of the data within that plane. The closer alignment of 45//45 and 45//-45 curves may imply that orientations with similar fibre angles exhibit similar damage progression behaviours, while the 0//0 orientation, with its distinct alignment, diverges from these patterns.

This orientation-based clustering within the same stress ratio plane points to a nuanced interaction between stress ratio and fibre orientation in determining crack growth behaviour. While the stress ratio appears to have the dominant effect, governing the plane of data alignment, the fibre orientation further modulates the data distribution within that plane. Specifically, orientations with similar fibre alignments tend to group closer together, suggesting that certain orientation pairings exhibit analogous crack progression characteristics. This finding could inform the design of composite materials by highlighting that specific fibre orientations, when subjected to identical stress ratios, yield comparable damage responses, potentially enhancing predictability in material performance across various configurations.

5.1.2. Exploration of Plane-Fitting Approaches for Stress Ratio Effects

The behaviour of the translated plots discussed in the previous section indicated that, for each stress ratio, the translated data points of G_{max} and $\Delta\sqrt{G}$ would lie on the same plane, regardless of the orientation of the plies in the composite. This observation led to the hypothesis that a single, common plane could capture the effect of stress ratio, as this behaviour did not align with any previously observed patterns.

The hypothesis proposed that a single plane equation could be derived to represent the data

across different stress ratios, allowing all data points to be described by one plane, irrespective of the specific stress ratio. However, visual inspection of the data and the proposed hypothesis revealed that, if such a plane were obtained, there would be a considerable amount of scatter perpendicular to it. This scatter would vary, with lower stress ratios exhibiting smaller deviations and higher stress ratios showing larger variations, indicating that the scatter around the proposed plane would not be uniform but would depend on both the data and the stress ratio.

To test this hypothesis, an initial approach was taken by attempting to fit a plane to the scatter data using three parameters: da/dN, G_{max}, and $\Delta\sqrt{G}$. Each of these parameters was linearized to create a linear plot, and the coefficients of the plane equation, along with the intercept, were determined. This plane was then plotted to evaluate the fit. As shown in Figure 5.17, the resulting plane provides a poor fit for the data across the different stress ratios, suggesting that further refinement of the model may be necessary.

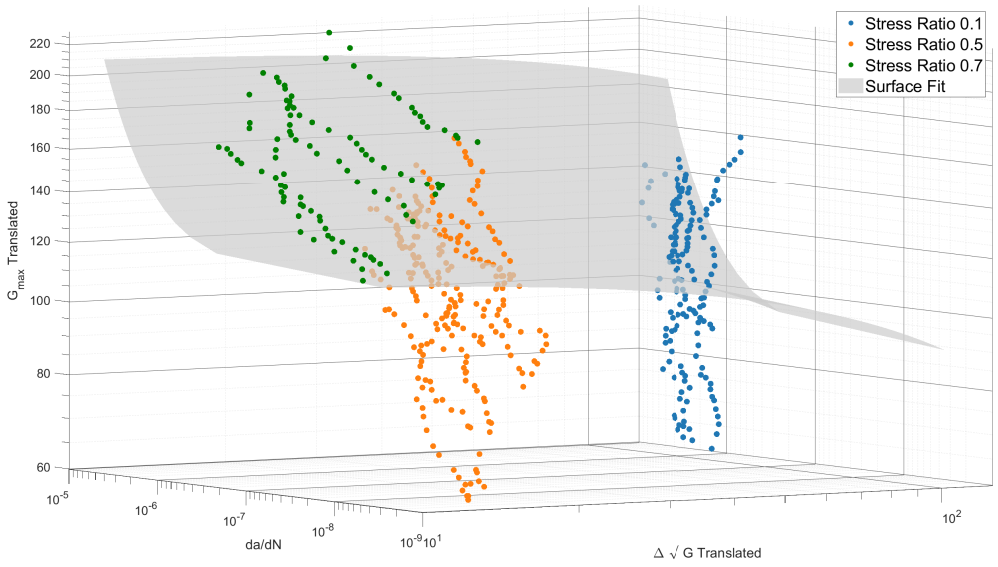

Figure 5.17: Plane Fit using Regression for Coefficient of the Plane Equation

Since the initial attempt was unsuccessful, the next approach involved adding a cross-term to the existing three parameters and performing regression with this modified model. This cross-term was introduced as the product of G_{max} and $\Delta\sqrt{G}$. The resulting plots are shown in Figure 5.18 and Figure 5.19.

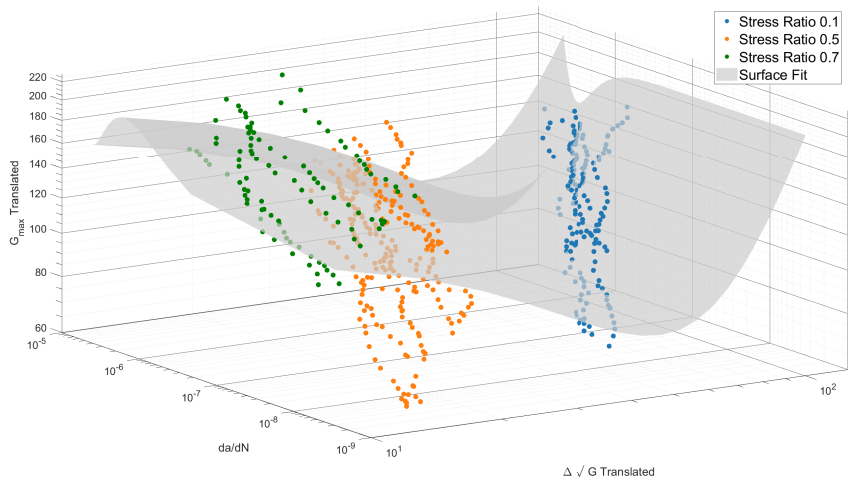

Figure 5.18: Plane Fit with additional Cross-Term

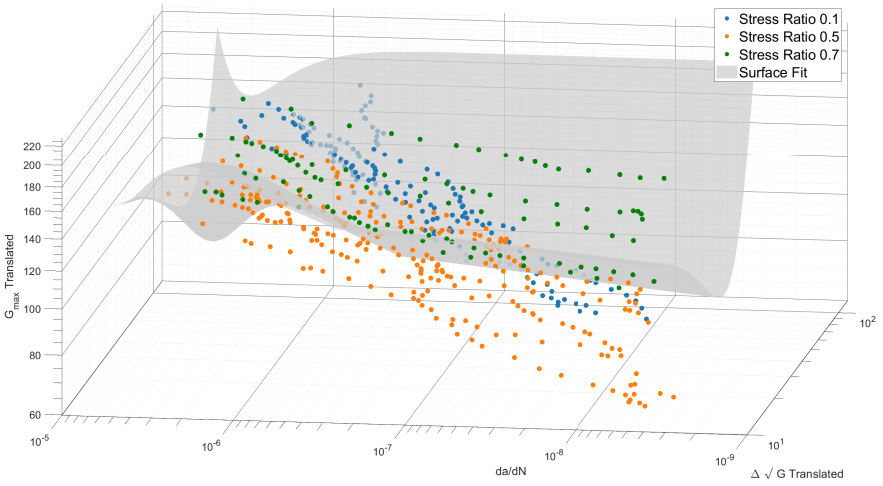

Figure 5.19: Surface Fit with Cross-Term

As observed in Figure 5.18, the fit with the cross-term is significantly improved compared to the previous attempt. However, Figure 5.19 reveals that the plane is slightly over-fitted, resulting in a noticeable kink at one end of the plane. This overfitting is problematic, as it indicates that the model may be too closely tailored to the specific data points, capturing noise rather than the underlying trend.

This kink suggests that the inclusion of the cross-term, while improving the overall fit, introduces artifacts that distort the plane's ability to generalize across different stress ratios. Further refinement may be needed, possibly by exploring alternative terms or constraining the model to reduce overfitting, to achieve a balance between accuracy and generalization.

The next approach involved manually enforcing a plane through the data, as the automated plane fitting had been unsuccessful in capturing the trend in the data points. This method

began with an initial line fit along the plane in which each specific data set lies. These line fits were then used to guide the fitting of a plane through the data. The resulting plane fit is shown in Figure 5.20 and Figure 5.21.

Although this approach produced a slightly better fit, it still fails to accurately capture the behaviour at the higher stress ratio of 0.7. This limitation suggests that the model may need further adjustments or additional parameters to better account for variations at higher stress ratios.

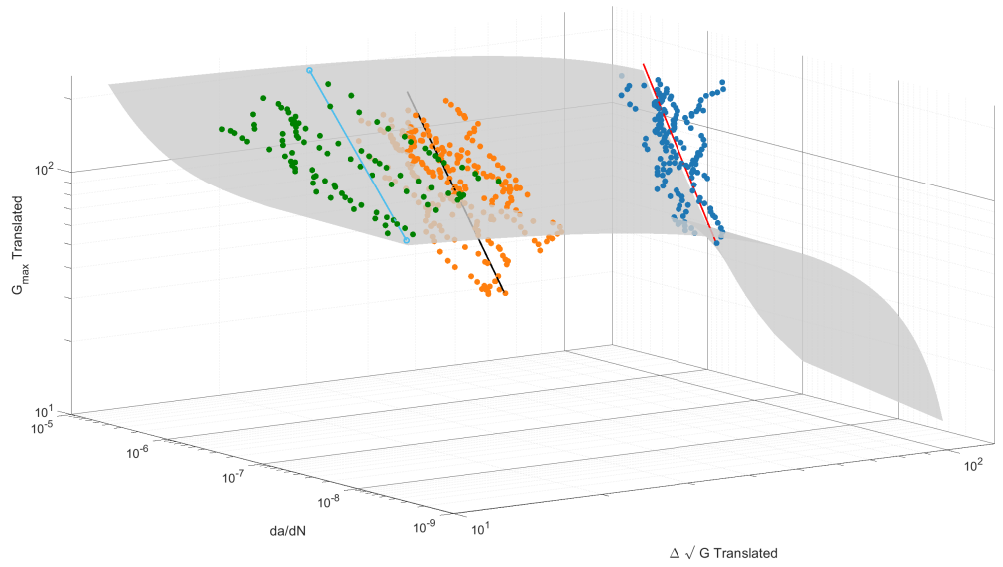

Figure 5.20: Forced Curve Fit

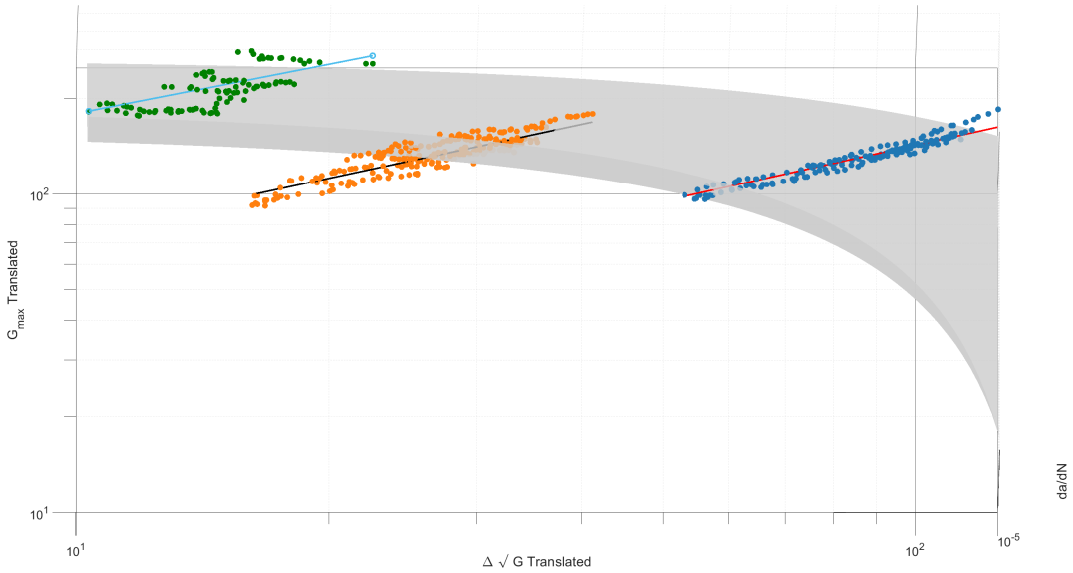

Figure 5.21: Forced Curve Fit

Subsequent attempts involved adopting a similar format to two-parameter models, with three specific formulations chosen and using translated parameters obtained from regression. The equations tested were as follows:

$$\frac{da}{dN} = B(\Delta G^{(1-\gamma)} G_{mean}^{\gamma})^m \tag{5.4}$$

$$\frac{da}{dN} = c(\sqrt{G_{max}} - \sqrt{G_{min}})^{2(1-\gamma)} G_{max}^{\gamma n} \tag{5.5}$$

$$\frac{da}{dN} = A(G_{max})^m + B(\Delta G)^n \tag{5.6}$$

However, a plane fit using these equations was also unsuccessful, as none of the fitted planes were able to capture the observed trend in the data. This was followed by an overall regression approach, where all data points were combined, and linear regression was performed to determine the coefficients for a plane fit. Unfortunately, this approach was also ineffective. All plots from these unsuccessful attempts are included in Appendix A.

5.2. Validation of the Regression Model Proposed

In this section, the accuracy and robustness of the proposed regression model are evaluated using two complementary validation methods. The first method involves translating the regression curve based on pre-crack lengths and comparing it with experimental results. This ensures that the experimental data consistently falls within the specified limits, thereby confirming the correct implementation of the model. The second validation assesses the influence of the data set size on the model's performance, providing insight into how the model responds to varying data volumes.

5.2.1. Comparison of Translated Regression Limits with Experimental Data

This validation step serves as a check to confirm the correct implementation of the method. The underlying concept is that if the translated zero-bridging curve is shifted back to match the specific pre-crack lengths of each specimen, the experimental data for that specimen should fall within the outer limits of the translated regression data. This ensures that the model has been implemented accurately in relation to the different pre-crack lengths.

This verification was done for Specimen 7 with the stress ratio of 0.1 and Specimen 12 with a stress ratio of 0.5 and is shown in Figure 5.22 and Figure 5.23 respectively.

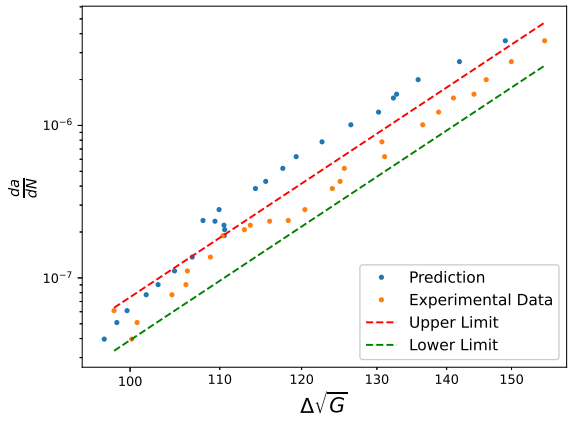

(a) Sequence 1

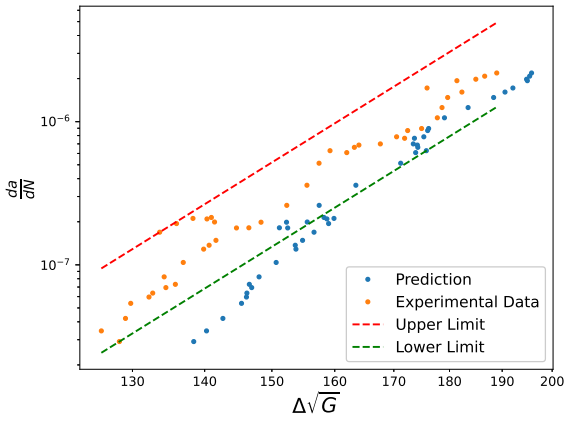

(b) Sequence 2

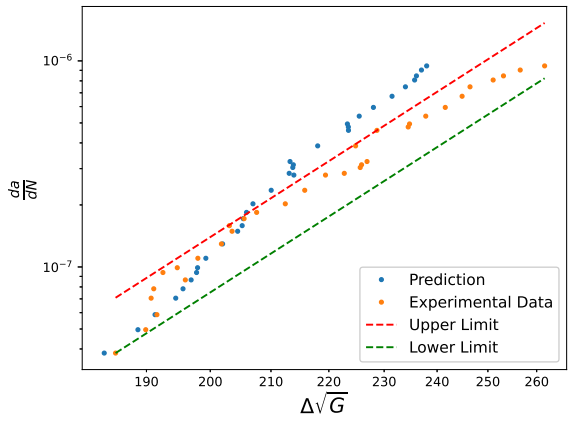

(c) Sequence 3

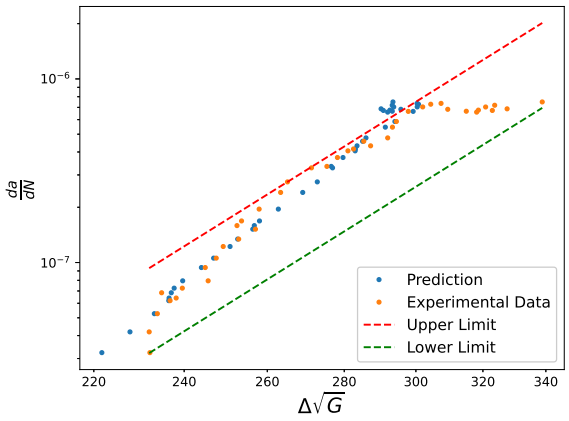

(d) Sequence 4

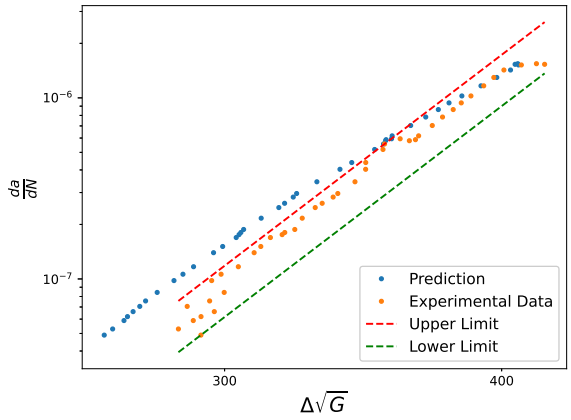

(e) Sequence 5

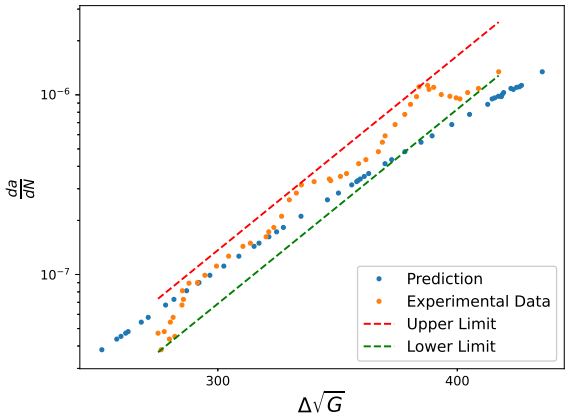

(f) Sequence 6

Figure 5.22: Prediction vs Experimental Data for Specimen 7

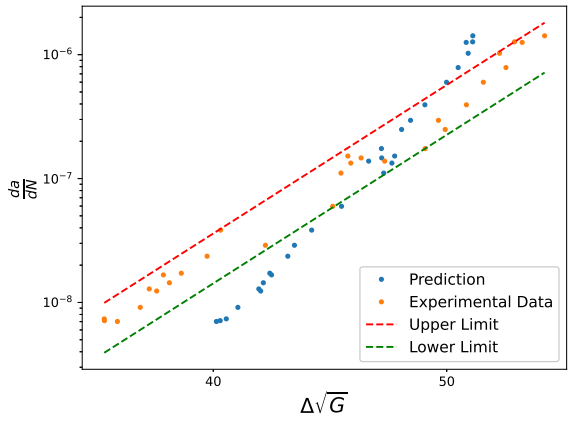

(a) Sequence 1

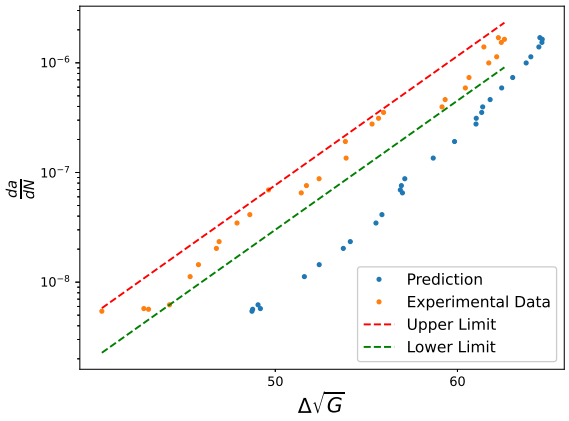

(b) Sequence 2

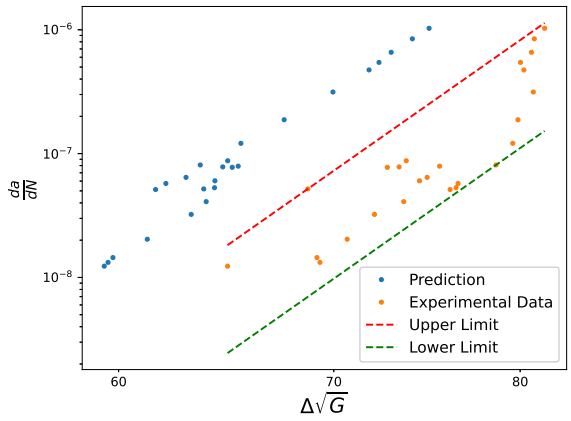

(c) Sequence 3

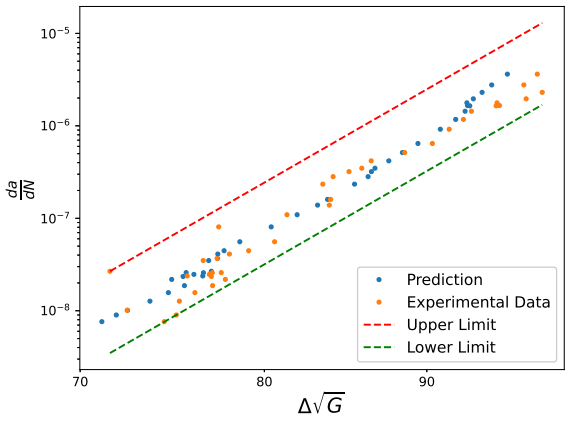

(d) Sequence 4

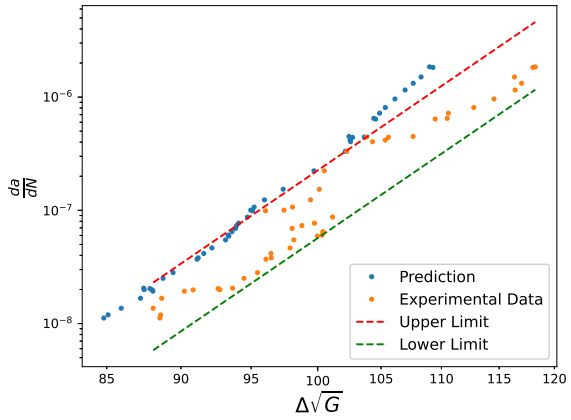

(e) Sequence 5

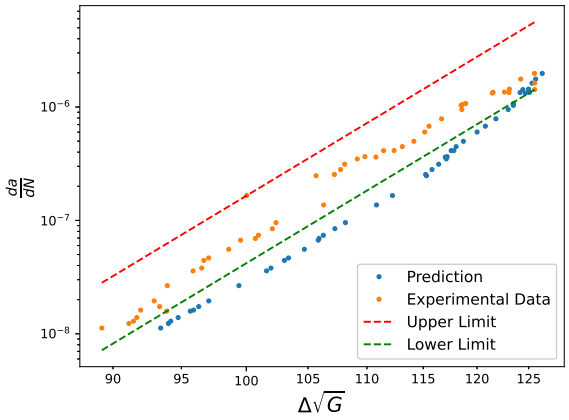

(f) Sequence 6

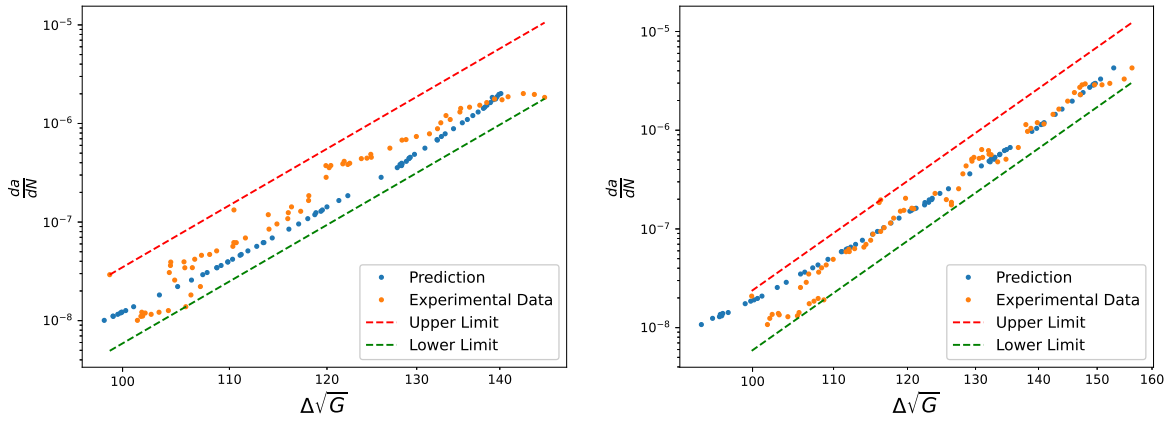

(g) Sequence 7

(h) Sequence 8

Figure 5.23: Prediction vs Experimental Data for Specimen 12

The translation plots above exhibit expected behaviour, with the predicted data points generally falling within the confidence intervals of the experimental data. This trend is consistently observed for both stress ratios, 0.1 and 0.5, demonstrating the validity of the methodology. However, an interesting anomaly arises in the earlier sequences—specifically, sequences 1 and 2 for specimen 7, and sequences 1, 2, and 3 for specimen 12—where the predicted curves fall outside the bounds of the confidence intervals. This deviation is not isolated, as a similar pattern was observed in other specimens analyzed in this study.

It is important to note that this behaviour is not indicative of an issue with the method's implementation. Instead, it reflects the inherent characteristics of the data translation process. The translation method relies on aligning the data across different sequences to ensure consistency, but in the earlier sequences, variations in the experimental data can amplify discrepancies.

As subsequent sequences align more closely with the predicted curves and conform to the confidence interval bounds, it becomes evident that this anomaly is restricted to the initial sequences. This suggests that the observed behaviour is a consequence of the data translation approach and its interaction with the natural variability in experimental data during the early stages of testing. Understanding and accounting for such trends can help refine future analyses, ensuring that early-sequence deviations do not undermine the overall reliability of the method.

5.2.2. Influence of Data Set Size on Model Performance

The plots generated in section 5.1 were developed using a regression method that incorporated both $\Delta\sqrt{G}$ and G_{max}. Alderliesten [42] established this regression methodology based on data from Specimen 7 and Specimen 11. Notably, these same specimens were also utilized by Yao et al. [40] in his exploration of the modified Paris relation. Alderliesten's analysis demonstrated an excellent correlation between the two specimens, which he further verified

through a comparison of their cumulative distribution functions. He observed that, apart from lower values of $\Delta\sqrt{G}$, there was strong agreement between the data from the two specimens.

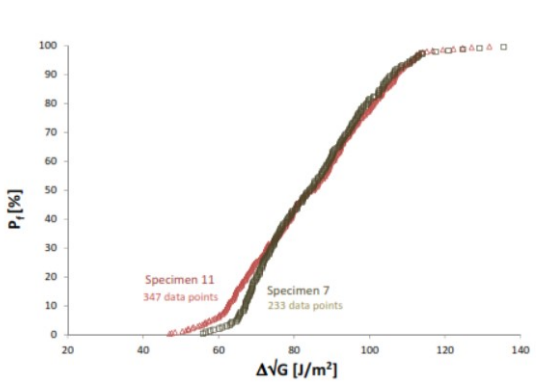

(a) Comparison between the cumulative density functions for specimen 7 and 11 by Alderliesten[42]

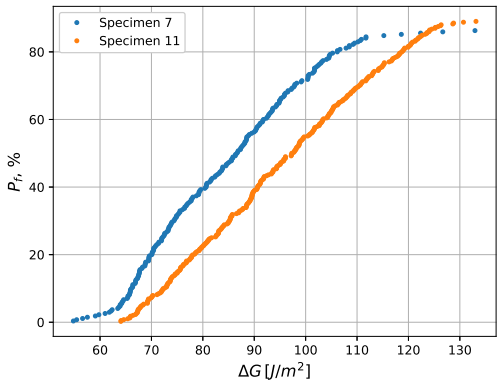

(b) Comparison between the cumulative density functions for specimen 7 and 11 using Python

Figure 5.24: Comparison between the cumulative density functions for specimens 7 and 11

However, this trend was not replicated in the analysis conducted using the code developed for this study. As illustrated in Figure 5.24, there is a significant difference between the two CDF plots. Upon further examination of the data components, a key distinction emerged between Alderliesten's analysis and the current study: the number of data points utilized for each specimen. In Alderliesten's work, Specimen 7 and Specimen 11 had 233 and 347 data points, respectively. In contrast, the present study increased the number of data points for these specimens to 269 and 391, respectively. This variation in dataset size may have contributed to the observed differences in the cumulative distribution functions, potentially impacting the accuracy and correlation of the results.

This dependence on the number of data points was also evident in the early stages of this study when the analysis was conducted manually in Excel, without the benefit of automation. During that phase, significant gaps in the data emerged, primarily due to the calculation of the crack growth rate, da/dN, using the 7-point polynomial method. These gaps were addressed by omitting the corresponding values from the dataset, resulting in a curve fitted through the remaining data points.

Interestingly, the correlation achieved in these early Excel-based analyses was significantly better, with the plots nearly overlapping. The curve derived from this manual process exhibited superior correlation compared to the plots published by Alderliesten. This improvement can be attributed to the number of data points used: in the manual analysis, Specimen 7 maintained the same 233 data points as in Alderliesten's published dataset, while Specimen 11 had only 307 data points, compared to Alderliesten's 347. This reduction in data points explains the enhanced correlation observed, even at lower $\Delta\sqrt{G}$ values.

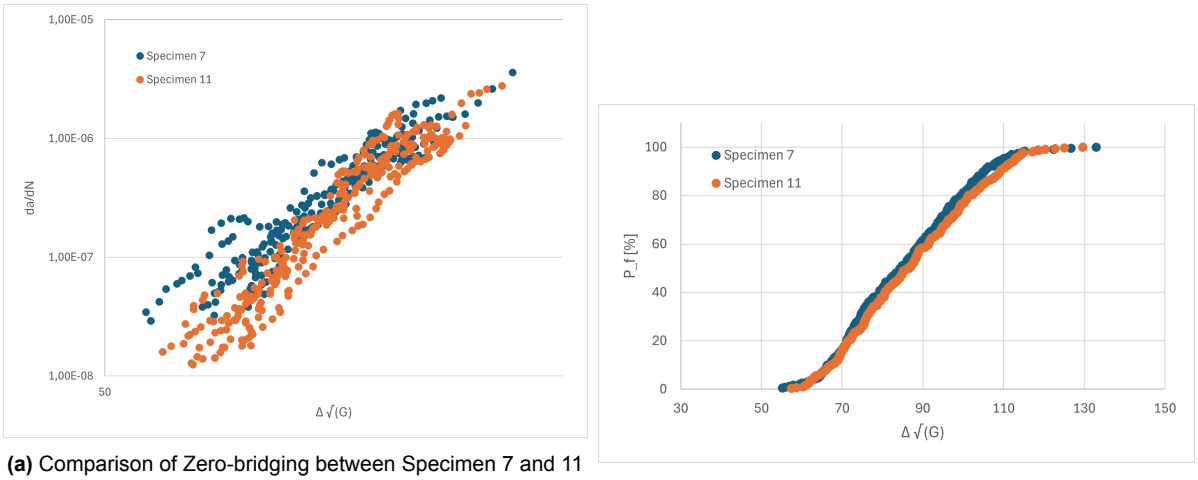

(a) Comparison of Zero-bridging between Specimen 7 and 11 using Excel

(b) Cumulative Distribution Function in Excel

Figure 5.25: Comparison of Zero-bridging and CDF plots using Excel

A similar cumulative distribution function was applied to the other data with different stress ratio and a similar trend was observed. The trend followed is similar to the one that is seen in Figure 5.24a with better correlation at lower $\Delta\sqrt{G}$ values.

Understanding the specific characteristics of the data being analyzed is fundamental, as this understanding directly influences the results obtained. Each software program has its own methodology for data analysis and approaches for handling exceptions or anomalies within the dataset. As illustrated in the preceding analysis, even when using the same dataset, different software can produce varied results due to these differing approaches.

For instance, variations in data pre-processing techniques, statistical algorithms, and the way each software interprets outliers or missing values can significantly affect the final outcomes. Ultimately, recognizing the nuances of data handling is essential for enhancing the reliability and validity of the results, enabling more effective comparisons across studies and promoting a deeper understanding of the underlying phenomena.

5.3. Comparison between Regression Method and Modified Paris Relation

In this study, the modified Paris relation proposed by Yao in [40] is plotted for comparison with the regression method developed. Yao applied a bi-linear fit to the combined data points from Specimen 7 and Specimen 11 to calculate G_{IC}. In an attempt to replicate Yao's approach, constraints were imposed on the curve to ensure that it passed through specified data points. However, despite these efforts, an exact replication of Yao's results was not achieved. Minor discrepancies were observed between the calculated values and those reported by Yao. These inconsistencies can be attributed to the inherent variability in applying bi-linear fits, which are highly sensitive to the choice of plotting methods or software.

This variability presents a significant challenge when trying to obtain consistent results. To mit-

igate these inconsistencies, polynomial fit methodology is explored, which offers more reliable and stable outcomes across different software and plotting techniques. Furthermore, since Yao's study used a combined dataset from both specimens for curve fitting, it is hypothesized that a more robust approach would involve fitting curves to each specimen's data individually. By following these guidelines, several fitting methodologies were implemented, and their results compared:

- Bi-Linear Fit by Yao
- Fitted Bi-Linear Model
- Individual Polynomial Fit for Specimen 7
- Individual Polynomial Fit for Specimen 11
- Combined Data Polynomial Fit

The aim of these methodologies was to ensure repeatability and consistent results across the different specimen analyses. A detailed comparison of the results from these various implementations is provided in Table 5.2, which lists key parameters, such as the length of the process zone, total strain energy release rate (SERR), and SERR at the crack tip.

	Length of Process Zone	**Total SERR**	**SERR Tip**
Bi-Linear Fit by Yao	62.980	631.150	162.760
Fitted Bi-Linear Model	71.577	584.434	166.217
Individual Polynomial Fit for Specimen 7	68.635	542.098	142.320
Individual Polynomial Fit for Specimen 11	100.848	614.123	128.000
Combined Data Polynomial Fit	100.848	611.982	135.155

Table 5.2: Comparison of Length of Process Zone, Total SERR, and SERR Tip across different fitting methods

5.3.1. Analysis of the Bi-Linear Fit by Yao

Yao's original approach utilized a bi-linear fit for the combined data of Specimen 7 and Specimen 11, resulting in a length of the process zone of 62.980 mm, a total SERR of 631.150 J/m^2 , and a crack tip SERR of 162.760 J/m^2. This approach provided a reasonable approximation of the material's fracture behaviour, but the methodology raises concerns regarding reproducibility due to its sensitivity to variations in curve fitting techniques and plotting software.

A re-implementation of the bi-linear model, with the addition of constraints to mimic the existing curve, yielded slightly different results, with a length of the process zone of 71.577 mm, a total SERR of 584.434 J/m^2, and a crack tip SERR of 166.217 J/m^2. The observed differences may be attributable to slight variations in the interpretation of the bi-linear segments or the method of data processing used in the re-implementation.

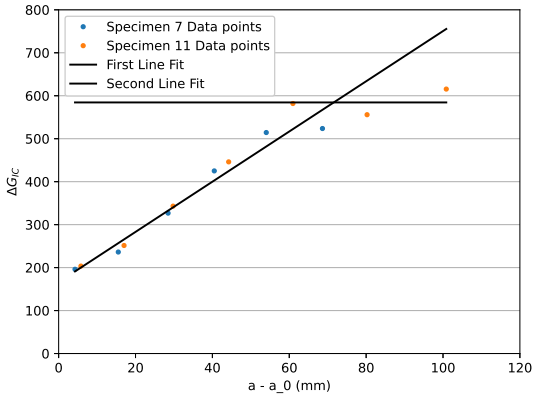

Figure 5.26: Bi-Linear Fit for R Curve

5.3.2. Polynomial Fit for Individual Specimens

Recognizing the limitations of the bi-linear fit, individual polynomial fits were applied to the data for each specimen. This method resulted in more consistent values for both Specimen 7 and Specimen 11. For Specimen 7, the polynomial fit produced a process zone length of 68.635 mm, a total SERR of 542.098 J/m^2, and a crack tip SERR of 142.320 J/m^2. For Specimen 11, the polynomial fit showed a process zone length of 100.848 mm, a total SERR of 614.123 J/m^2, and a crack tip SERR of 128.000 J/m^2. These values are more stable and reproducible as compared to the bi-linear fit.

The corresponding R-curves for the individual polynomial fits are shown in Figure 5.27. It can be observed that the polynomial fit provides a smoother and more continuous representation of the fracture process compared to the abrupt transitions seen in the bi-linear fits.

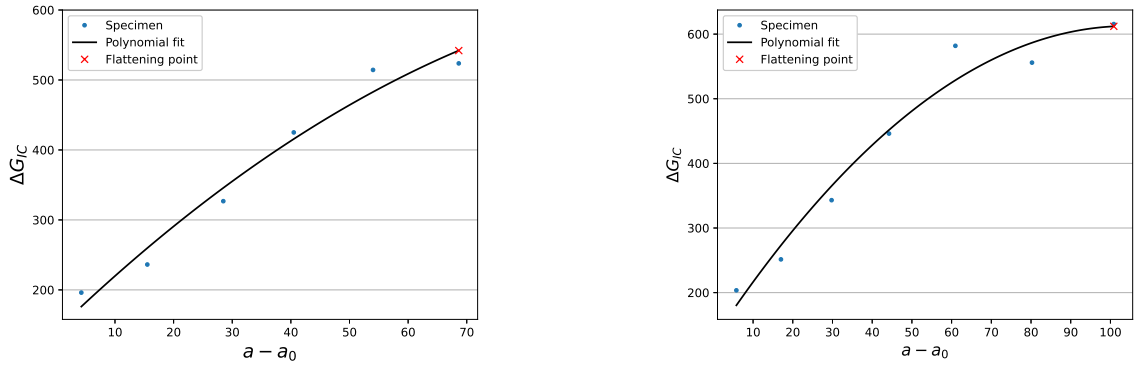

(a) Polynomial R Curve for Specimen 7

(b) Polynomial R Curve for Specimen 11

Figure 5.27: Individual Polynomial R Curve fits for Specimen 7 and Specimen 11

5.3.3. Polynomial Fit for Combined Data

A polynomial fit was also applied to the combined data from Specimen 7 and Specimen 11 to assess the impact of using aggregate data as seen in Figure 5.28. The results of this fit, as

shown in Table 5.2, reveal a process zone length of 100.848 mm, a total SERR of 611.982 J/m^2, and a crack tip SERR of 135.155 J/m^2. While this combined fit closely matches the polynomial fit for Specimen 11, it significantly diverges from the polynomial fit for Specimen 7. This discrepancy suggests that combining data from different specimens into a single fit may obscure important specimen-specific fracture behaviour, leading to skewed results.

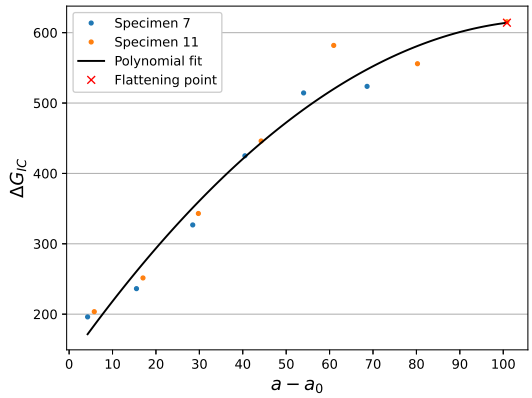

Figure 5.28: Polynomial R Curve fit for Specimen 7 and 11 combined

5.3.4. Comparison of Fitting Methods

The results of the different fitting methods are visually compared in the R-curve plots for Specimen 7 and Specimen 11. Figures 5.29, 5.30, and 5.32 show the comparison between Yao's modified Paris relation using the different fitting approaches applied in this study and the regression method used in this study. The differences in the R-curves from the regression method which is taken as the benchmark highlights the inconsistencies introduced by the bi-linear fit, particularly for Specimen 7.

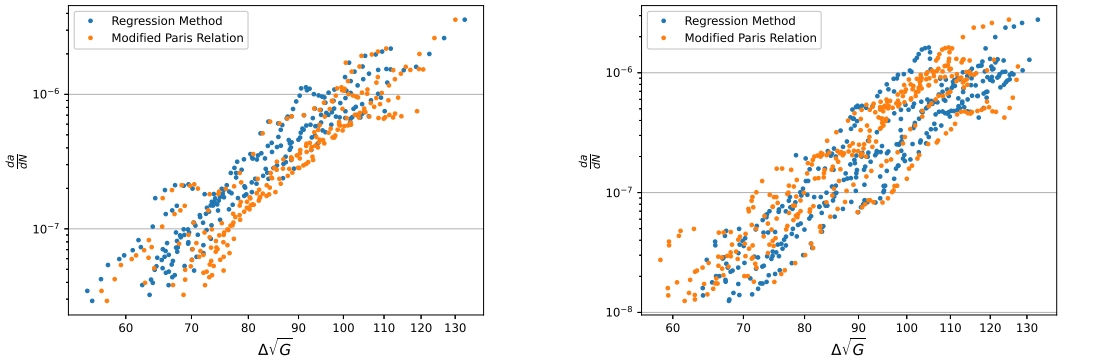

(a) Regression and Modified Paris Relation Comparison for Specimen 7

(b) Regression and Modified Paris Relation Comparison for Specimen 11

Figure 5.29: Regression and Modified Paris Relation Comparison for Specimen 7 and Specimen 11 from Paper

A more substantial difference was observed when the bi-linear fit implemented in this study

was compared with the regression method, as shown in Figure 5.30. For Specimen 7, the difference between the two methods is particularly pronounced, with significant variation in the SERR values, highlighting the limitations of the bi-linear approach in capturing the detailed fracture process.

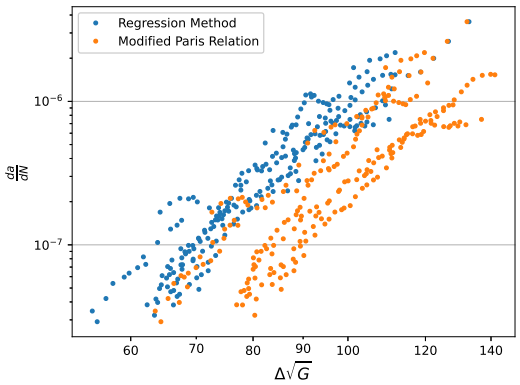

(a) Regression and Modified Paris Relation Comparison for Specimen 7 using Bi-Linear Fit

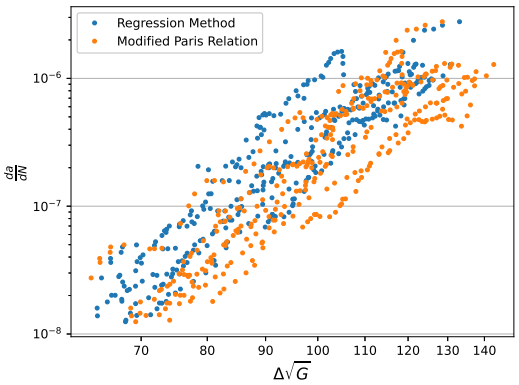

(b) Regression and Modified Paris Relation Comparison for Specimen 11 using Bi-Linear Fit

Figure 5.30: Regression and Modified Paris Relation Comparison for Specimen 7 and Specimen 11 using Bi-Linear Fit

Conversely, using the polynomial fit on individual specimen data, as shown in Figure 5.32, resulted in better agreement between the Zero Bridging method and the polynomial fit for both specimens, with only minor differences observed for Specimen 7 along the x-axis.

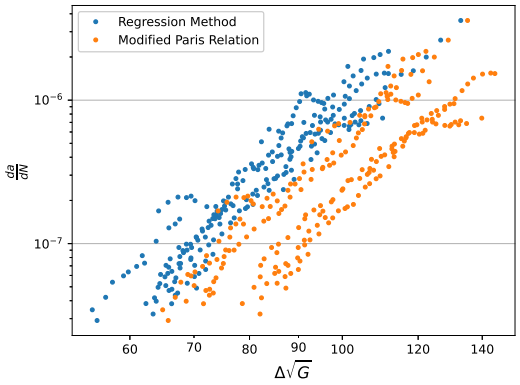

(a) Regression and Modified Paris Relation Comparison for Specimen 7 using Combined Polynomial Fit

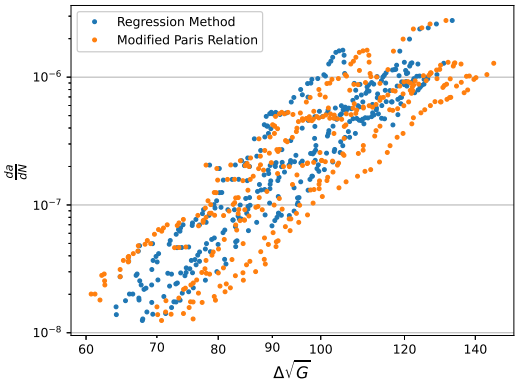

(b) Regression and Modified Paris Relation Comparison for Specimen 11 using Combined Polynomial Fit

Figure 5.31: Regression and Modified Paris Relation Comparison for Specimen 7 and Specimen 11 using Combined Polynomial Fit

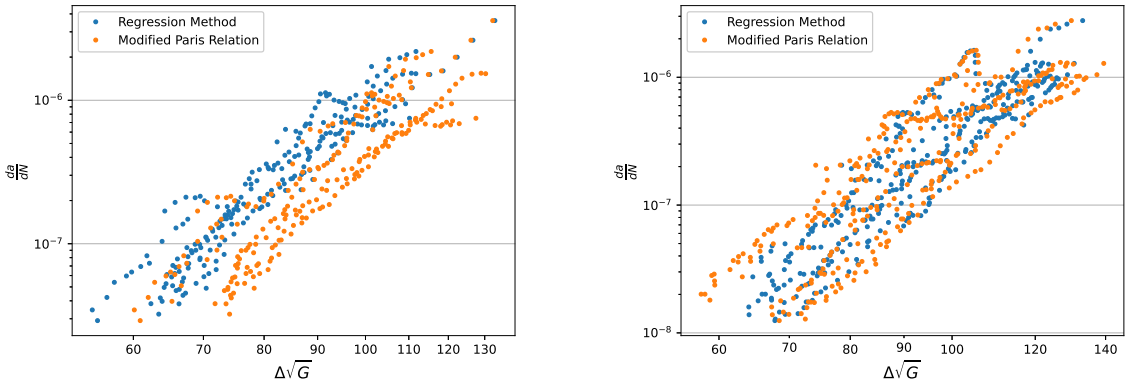

(a) Regression and Modified Paris Relation Comparison for Specimen 7 using Individual Polynomial Fit

(b) Regression and Modified Paris Relation Comparison for Specimen 11 using Individual Polynomial Fit

Figure 5.32: Regression and Modified Paris Relation Comparison for Specimen 7 and Specimen 11 using Individual Polynomial Fit

5.3.5. Analysis and Recommendations

The results of this study demonstrate that the use of a bi-linear fit, as employed by Yao, introduces significant variability and inconsistency in the analysis of delamination crack growth. This variability stems from the sensitivity of the bi-linear fit to the specific plotting methods used, as well as the choice of data points for the bi-linear segments. Though the values proposed by Yao provided a good correlation between the regression data and the modified Paris relation the inability to reproduce those values makes the methodology difficult to standardize.

In contrast, polynomial fits offer a more robust and reliable approach for analyzing individual specimens. The polynomial fit provides a smoother and more continuous representation of the R-curve, better capturing the gradual changes in energy release rate and crack growth. Moreover, applying polynomial fits to individual specimens avoids the pitfalls of combining data from multiple specimens, which can obscure important specimen-specific behaviour.

Based on the analysis presented in this study, it is recommended that future studies avoid using bi-linear fits and instead adopt second degree polynomial fits for analyzing fracture processes. Furthermore, each specimen's data should be analyzed independently, as combining data from different specimens can lead to unrepresentative results.

6

Conclusion

Composites have become integral to aircraft primary structures, but as design and testing methodologies advance, the current certification processes have grown increasingly complex and costly. Transitioning to a simpler and more efficient certification framework requires adapting testing methods to make them more representative of real-life conditions. A prime example is fatigue delamination testing for fibre-reinforced composites, where a standardized testing protocol is lacking. The absence of consensus on an appropriate similitude parameter for characterizing fatigue delamination growth presents a significant obstacle. This issue is largely attributed to fibre bridging, a phenomenon that introduces variability in test data, making it difficult to establish a standardized approach. This presents a significant issue, as fibre bridging is a phenomenon that primarily occurs during testing and very rarely extend to real-world structural applications. Consequently, reliance on fibre bridging effects in testing could lead to underdesign, as fibre bridging is known to enhance the toughness of composites and significantly slow down the delamination process.

The aim of this thesis was to develop an ISO standard for Mode I fatigue delamination testing in fibre-reinforced polymer composites. This included determining the most suitable similitude parameter to characterize delamination growth while accounting for fibre bridging effects. Through this work, various potential parameters were evaluated to identify the one that best represents delamination growth. For addressing fibre bridging, existing methods—such as the modified Paris relation and regression techniques—were analyzed to determine their advantages and limitations, ultimately aiming to select the most reliable data processing method. A Python code was developed to analyze raw test data and perform calculations for both methods. Given Python's limitations in 3D plot visualization, a MATLAB version of the code was also created to facilitate improved viewing of generated plots.

The thesis initially implements the zero-bridging method, as this approach shows promise for use in standardization. Analyses were conducted separately for the two parameters, $\Delta\sqrt{G}$

and G_{max}, applying the regression equation individually to each and generating respective plots. Observations from these plots, combined with insights from literature, highlighted the importance of accurately characterizing both monotonic and cyclic load components for a comprehensive understanding of delamination growth behaviour. Here, G_{max} represents the monotonic load component, while $\Delta\sqrt{G}$ captures the cyclic component. These findings led to the conclusion that 3D plots incorporating both parameters and the delamination growth rate (da/dN) provide the most complete perspective. These 3D plots revealed that, for a constant stress ratio, the translated data points lie on the same plane, while variations in stress ratio result in shifts to different planes. Traditional models that focus solely on either cyclic or monotonic loading often overlook the complex interplay between these components, which is crucial for describing delamination behaviour in FRPs. This study demonstrates that incorporating both components in predictive equations is essential to capture their combined influence on crack growth rates, especially in cases with significant fibre bridging. These curves allow for a clear representation of delamination progression without the confounding effects of fibre bridging, thereby providing a reliable methodology for analyzing fatigue delamination growth.

An additional aspect of the zero-bridging curve that remained largely unexplored using the regression method was the influence of varying fibre orientations on its behaviour. Although data on this was limited, three orientations— 0//0, 45//45, and 45//-45 —were analyzed. In the resulting 3D plot, similar to previous cases, it was observed that orientation did not affect the plane in which data points lay, as long as the stress ratio remained constant. However, it was noted that the data points for 45//45 and 45//-45 orientations were closer to each other than to the 0//0 orientation, though they did not overlap. This suggests that similar orientations exhibit comparable delamination behaviour, indicating that orientation plays a role in influencing delamination patterns without altering the stress ratio-dependent plane.

A key drawback, highlighted in the literature and observed in this thesis, is the need for multiple delamination resistance curves per specimen to effectively apply this method. This requirement poses a challenge for existing datasets, where most specimens have only a single delamination resistance curve, making it difficult to implement this methodology. As discussed by Alderliesten[42], this limitation can be addressed using an alternative approach—the modified Paris relation proposed by Yao et al. [40]. Both the literature and this thesis confirm that the curve generated by the modified Paris relation closely resembles the one produced through the regression method. However, a significant drawback of the modified Paris relation is the bi-linear fit proposed in Yao's initial work [40]. This thesis examines the limitations of this approach and suggests a polynomial fit through individual data points as a more consistent and reproducible alternative. This alternative approach, along with the automation of zero-bridging curve plotting using the modified Paris relation, is implemented in the Python code developed for this study.

7

Recommendation for Future Work

This chapter outlines key recommendations for future work based on the methodology developed in this thesis. A code was developed in both Python and MATLAB to automate the implementation of the regression method and the modified Paris relation for analyzing fatigue delamination behaviour. While the current version of the code is detailed and comprehensive, future improvements could focus on enhancing coding practices and simplifying function structures. Refining these aspects would improve the code's readability, maintainability, and efficiency, making it more accessible for further research and practical applications in fatigue analysis of fibre-reinforced composites.

A significant challenge that remained unresolved was the development of an equation capable of accounting for the effect of stress ratio on delamination behaviour. As outlined in chapter 5, various attempts were made to identify a plane that could accurately capture the observed trends when plotting data for different stress ratios. The approaches explored and their corresponding results are presented in chapter 5 and Appendix A.

Given these challenges, the next course of action could focus on identifying an equation that defines a plane capable of fitting data across the different stress ratios, thereby accounting for the stress ratio effect and enabling the development of a unified predictive model. This approach could involve exploring alternative fitting techniques or adjustments to existing two-parameter models to achieve a more accurate representation. Developing such a combined equation would be a significant step toward a more comprehensive understanding of the influence of stress ratio on delamination behaviour.

References

[1] Rafiullah Khan. “Delamination growth in composites under fatigue loading”. In: (2013).

[2] William G Roeseler et al. “Composite structures: the first 100 years”. In: *16th International Conference on Composite Materials*. Japan Society for Composite Materials Kyoto, Japan. 2007, pp. 1–41.

[3] SA Chisholm et al. “Forty Years of Structural Durability and Damage Tolerance at Boeing Commercial Airplanes”. In: *Boeing Technical Journal* 6.3 (2016).

[4] J Rouchon and MJ Bos. “Fatigue and damage tolerance evaluation of structures: the composite materials response”. In: (2009).

[5] Federal Aviation Authority. *Airworthiness Advisory Circular No: 20-107B. Composite Aircraft Structure*. 2009.

[6] John-Alan Pascoe, René Alderliesten, and R. Benedictus. “Methods for the Prediction of Fatigue Delamination Growth in Composites and Adhesive Bonds - A Critical Review”. In: *Engineering Fracture Mechanics* 112-113 (Oct. 2013), pp. 72–96. DOI: 10.1016/j.engfracmech.2013.10.003.

[7] D. R. Atodaria, S. K. Putatunda, and P. K. Mallick. “Delamination Growth Behavior of a Fabric Reinforced Laminated Composite Under Mode I Fatigue”. In: *Journal of Engineering Materials and Technology* 121.3 (July 1999), pp. 381–385. ISSN: 0094-4289. DOI: 10.1115/1.2812390. eprint: https://asmedigitalcollection.asme.org/materialstechnology/article-pdf/121/3/381/5528582/381_1.pdf. URL: https://doi.org/10.1115/1.2812390.

[8] Norbert Blanco et al. “Mixed-mode delamination growth in carbon–fibre composite laminates under cyclic loading”. In: *International Journal of Solids and Structures* 41 (July 2004), pp. 4219–4235. DOI: 10.1016/j.ijsolstr.2004.02.040.

[9] A.J. Brunner, N. Murphy, and G. Pinter. “Development of a standardized procedure for the characterization of interlaminar delamination propagation in advanced composites under fatigue mode I loading conditions”. In: *Engineering Fracture Mechanics* 76.18 (2009). Fracture of Polymers, Composites and Adhesives, pp. 2678–2689. ISSN: 0013-7944. DOI: https://doi.org/10.1016/j.engfracmech.2009.07.014. URL: https://www.sciencedirect.com/science/article/pii/S0013794409002392.

[10] Masaki Hojo et al. “Effect of stress ratio on near-threshold propagation of delimination fatigue cracks in unidirectional CFRP”. In: *Composites Science and Technology* 29.4 (1987), pp. 273–292. ISSN: 0266-3538. DOI: https://doi.org/10.1016/0266-3538(87)90076-5. URL: https://www.sciencedirect.com/science/article/pii/0266353887900765.

[11] Masaki Hojo et al. “Mode I delamination fatigue properties of interlayer-toughened CF/epoxy laminates”. In: *Composites Science and Technology* 66.5 (2006). Reliability and Life Prediction of Composite Structures, pp. 665–675. ISSN: 0266-3538. DOI: https://doi.org/10.1016/j.compscitech.2005.07.038. URL: https://www.sciencedirect.com/science/article/pii/S0266353805003180.

[12] R. Jones, A.J. Kinloch, and W. Hu. “Cyclic-fatigue crack growth in composite and adhesively-bonded structures: The FAA slow crack growth approach to certification and the problem of similitude”. In: *International Journal of Fatigue* 88 (2016), pp. 10–18. ISSN: 0142-1123. DOI: https://doi.org/10.1016/j.ijfatigue.2016.03.008. URL: https://www.sciencedirect.com/science/article/pii/S0142112316300135.

[13] Atsushi Hosoi et al. “High-cycle fatigue characteristics of quasi-isotropic CFRP laminates”. In: *Advanced Composite Materials - ADV COMPOS MATER* 16 (Mar. 2007), pp. 151–166. DOI: 10.1163/156855107780918964.

[14] Davide Tumino and F. Cappello. “Simulation of Fatigue Delamination Growth in Composites with Different Mode Mixtures”. In: *Journal of Composite Materials - J COMPOS MATER* 41 (Oct. 2007), pp. 2415–2441. DOI: 10.1177/0021998307075439.

[15] Z. Suo, G. Bao, and B. Fan. “Delamination R-curve phenomena due to damage”. In: *Journal of the Mechanics and Physics of Solids* 40.1 (1992), pp. 1–16. ISSN: 0022-5096. DOI: https://doi.org/10.1016/0022-5096(92)90198-B. URL: https://www.sciencedirect.com/science/article/pii/002250969290198B.

[16] Bent F Sørensen and Torben K Jacobsen. “Large-scale bridging in composites: R-curves and bridging laws”. In: *Composites Part A: Applied Science and Manufacturing* 29.11 (1998), pp. 1443–1451. ISSN: 1359-835X. DOI: https://doi.org/10.1016/S1359-835X(98)00025-6. URL: https://www.sciencedirect.com/science/article/pii/S1359835X98000256.

[17] T.K. Jacobsen and B.F. Sørensen. “Mode I intra-laminar crack growth in composites — modelling of R-curves from measured bridging laws”. In: *Composites Part A: Applied Science and Manufacturing* 32.1 (2001), pp. 1–11. ISSN: 1359-835X. DOI: https://doi.org/10.1016/S1359-835X(00)00139-1. URL: https://www.sciencedirect.com/science/article/pii/S1359835X00001391.

[18] Carlos Dávila, Cheryl Rose, and Pedro Camanho. “A procedure for superposing linear cohesive laws to represent multiple damage mechanisms in the fracture of composites”. In: *International Journal of Fracture* 158 (Aug. 2009), pp. 211–223. DOI: 10.1007/s10704-009-9366-z.

[19] Alessandro Airoldi and Carlos Dávila. “Identification of material parameters for modelling delamination in the presence of fibre bridging”. In: *Composite Structures* 94 (Nov. 2012), pp. 3240–3249. DOI: 10.1016/j.compstruct.2012.05.014.

[20] Bryan Harris. “A historical review of the fatigue behaviour of fibre-reinforced plastics”. In: *Fatigue in composites* (2003), pp. 3–35.

[21] J. Schijve. *Fatigue of Structures and Materials*. Springer Netherlands, 2001. ISBN: 9780792370147. URL: https://books.google.nl/books?id=Xjy5khx4Mo0C.

[22] Daniel Marcus Gleich. “Stress analysis of structural bonded joints”. In: (2002).

[23] Calvin Rans, René Alderliesten, and Rinze Benedictus. “Misinterpreting the results: How similitude can improve our understanding of fatigue delamination growth”. In: *Composites Science and Technology* 71.2 (2011), pp. 230–238.

[24] Anthony Kinloch et al. “Delamination Growth in Polymer-Matrix Fibre Composites and the Use of Fracture-Mechanics Data for Material Characterization and Life Prediction”. In: Jan. 2018, pp. 763–798. ISBN: 978-0-08-100540-08. DOI: 10.1016/B978-0-08-100540-8.00013-3.

[25] R. Jones, W. Hu, and A. J. Kinloch. “A convenient way to represent fatigue crack growth in structural adhesives”. In: *Fatigue & Fracture of Engineering Materials & Structures* 38.4 (2015), pp. 379–391. DOI: https://doi.org/10.1111/ffe.12241. eprint: https://onlinelibrary.wiley.com/doi/pdf/10.1111/ffe.12241. URL: https://onlinelibrary.wiley.com/doi/abs/10.1111/ffe.12241.

[26] R. Jones et al. “Crack growth in adhesives: Similitude and the Hartman-Schijve equation”. In: *Composite Structures* 273 (2021), p. 114260. ISSN: 0263-8223. DOI: https://doi.org/10.1016/j.compstruct.2021.114260. URL: https://www.sciencedirect.com/science/article/pii/S0263822321007224.

[27] Yu Gong et al. “A novel model for determining the fatigue delamination resistance in composite laminates from a viewpoint of energy”. In: *Composites Science and Technology* 167 (2018), pp. 489–496.

[28] Rafiullah Khan et al. “Effect of stress ratio or mean stress on fatigue delamination growth in composites: critical review”. In: *Composite Structures* 124 (2015), pp. 214–227.

[29] Claes-Göran Gustafson and Masaki Hojo. “Delamination fatigue crack growth in unidirectional graphite/epoxy laminates”. In: *Journal of Reinforced Plastics and Composites* 6.1 (1987), pp. 36–52.

[30] Masaki Hojo et al. “Effect of stress ratio on near-threshold propagation of delimination fatigue cracks in unidirectional CFRP”. In: *Composites Science and Technology* 29.4 (1987), pp. 273–292.

[31] S Mall, G Ramamurthy, and MA Rezaizdeh. “Stress ratio effect on cyclic debonding in adhesively bonded composite joints”. In: *Composite structures* 8.1 (1987), pp. 31–45.

[32] Liaojun Yao et al. “A validation of a modified Paris relation for fatigue delamination growth in unidirectional composite laminates”. In: *Composites Part B: Engineering* 132 (2018), pp. 97–106. ISSN: 1359-8368. DOI: https://doi.org/10.1016/j.compositesb.2017.09.007. URL: https://www.sciencedirect.com/science/article/pii/S1359836816329067.

[33] DR Atodaria, SK Putatunda, and PK Mallick. “A fatigue crack growth model for random fiber composites”. In: *Journal of Composite Materials* 31.18 (1997), pp. 1838–1855.

[34] DR Atodaria, SK Putatunda, and PK Mallick. “Fatigue crack growth model and mechanism of a random fiber SMC composite”. In: *Polymer composites* 20.2 (1999), pp. 240–249.

[35] DR Atodaria, SK Putatunda, and PK Mallick. “Delamination growth behavior of a fabric reinforced laminated composite under mode I fatigue”. In: (1999).

[36] Junhui Jia and Julio F Davalos. “Study of load ratio for mode-I fatigue fracture of wood-FRP-bonded interfaces”. In: *Journal of composite materials* 38.14 (2004), pp. 1211–1230.

[37] Rafiullah Khan, René Alderliesten, and Rinze Benedictus. “Two-parameter model for delamination growth under mode I fatigue loading (Part A: Experimental study)”. In: *Composites Part A: Applied Science and Manufacturing* 65 (2014), pp. 192–200.

[38] Rafiullah Khan, René Alderliesten, and Rinze Benedictus. “Two-parameter model for delamination growth under mode I fatigue loading (Part B: Model development)”. In: *Composites Part A: Applied Science and Manufacturing* 65 (2014), pp. 201–210.

[39] Liaojun Yao et al. “Temperature effects on fatigue delamination behavior in thermoset composite laminates”. In: *Engineering Fracture Mechanics* 295 (Dec. 2023), p. 109799. DOI: 10.1016/j.engfracmech.2023.109799.

[40] Liaojun Yao et al. “A modified Paris relation for fatigue delamination with fibre bridging in composite laminates”. In: *Composite Structures* 176 (2017), pp. 556–564.

[41] Masaki Hojo et al. “Modes I and II interlaminar fracture toughness and fatigue delamination of CF/epoxy laminates with self-same epoxy interleaf”. In: *International journal of fatigue* 28.10 (2006), pp. 1154–1165.

[42] René Alderliesten. “Fatigue delamination of composite materials: Approach to exclude large scale fibre bridging”. English. In: *IOP Conference Series: Materials Science and Engineering* 388.1 (July 2018). ISSN: 1757-8981. DOI: 10.1088/1757-899X/388/1/012002.

[43] Rafiullah Khan. “Fiber bridging in composite laminates: a literature Review”. In: *Composite Structures* 229 (Sept. 2019), p. 111418. DOI: 10.1016/j.compstruct.2019.111418.

[44] Shin-ichi Takeda, Yoji Okabe, and Nobuo Takeda. “Delamination detection in CFRP laminates with embedded small-diameter fiber Bragg grating sensors”. In: *Composites Part A: Applied Science and Manufacturing* 33 (July 2002), pp. 971–980. DOI: 10.1016/S1359-835X(02)00036-2.

[45] RC Alderliesten. “How proper similitude can improve our understanding of crack closure and plasticity in fatigue”. In: *International Journal of Fatigue* 82 (2016), pp. 263–273.

[46] Liaojun Yao et al. “Discussion on the use of the strain energy release rate for fatigue delamination characterization”. In: *Composites Part A: Applied Science and Manufacturing* 66 (2014), pp. 65–72.

[47] Rhys Jones, Anthony J Kinloch, and Wenchen Hu. “Cyclic-fatigue crack growth in composite and adhesively-bonded structures: The FAA slow crack growth approach to certification and the problem of similitude”. In: *International Journal of Fatigue* 88 (2016), pp. 10–18.

[48] Z Suo, G Bao, and B Fan. “Delamination R-curve phenomena due to damage”. In: *Journal of the Mechanics and Physics of Solids* 40.1 (1992), pp. 1–16.

[49] G Bao and Z Suo. “Remarks on crack-bridging concepts”. In: (1992).

[50] MJ Donough et al. “Scaling parameter for fatigue delamination growth in composites under varying load ratios”. In: *Composites Science and Technology* 120 (2015), pp. 39–48.

[51] L Yao. “Mode I fatigue delamination growth in composite laminates with fibre bridging”. In: (2015).

A

Unsuccessful Plane Fits

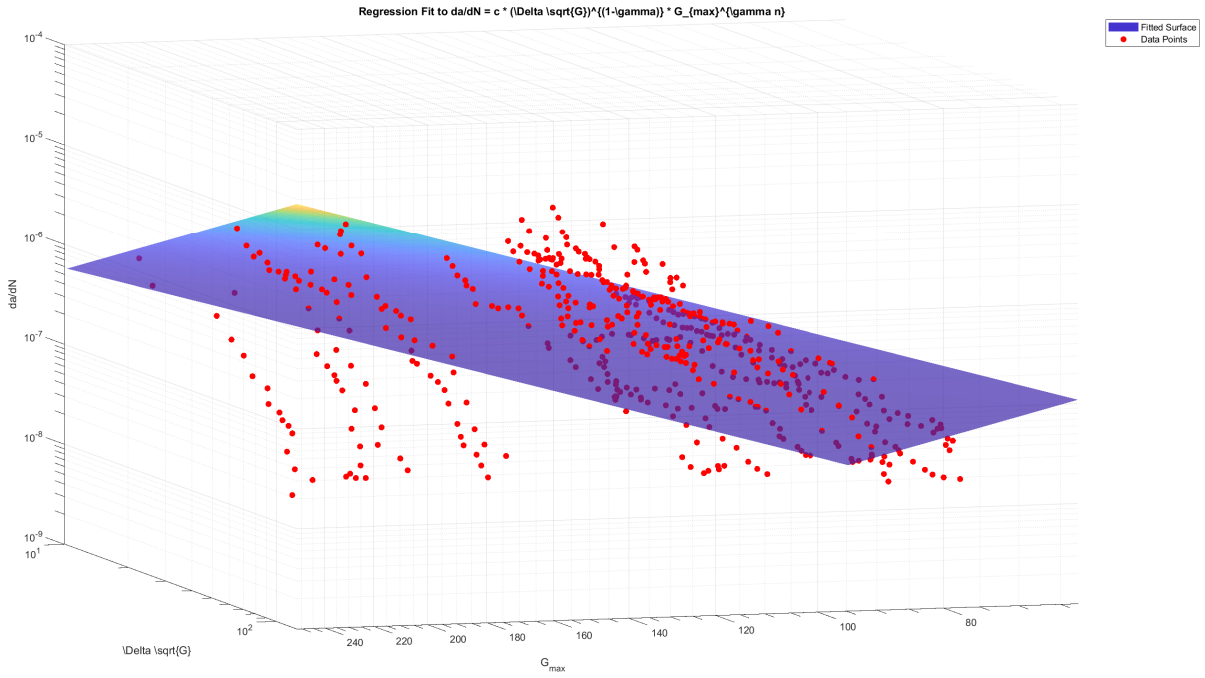

Figure A.1: Plane Fit using Hojo's two parameter model

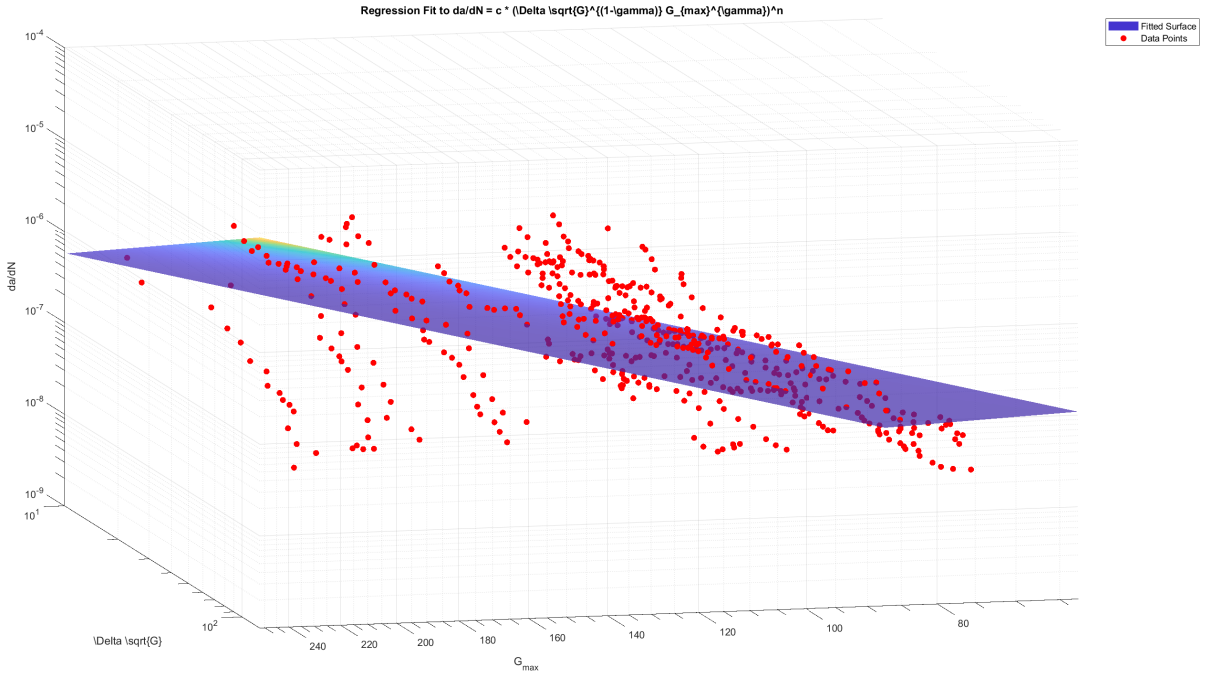

Figure A.2: Plane Fit using Jia's two parameter model

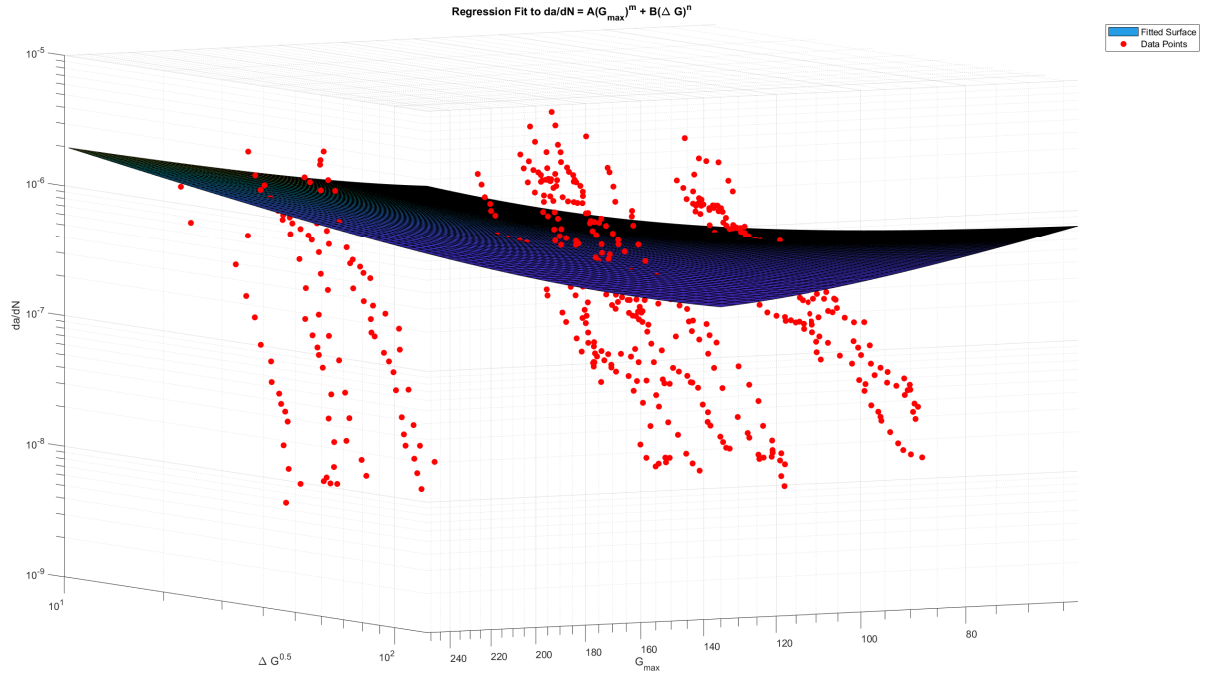

Figure A.3: Plane Fit using Khan's two parameter model

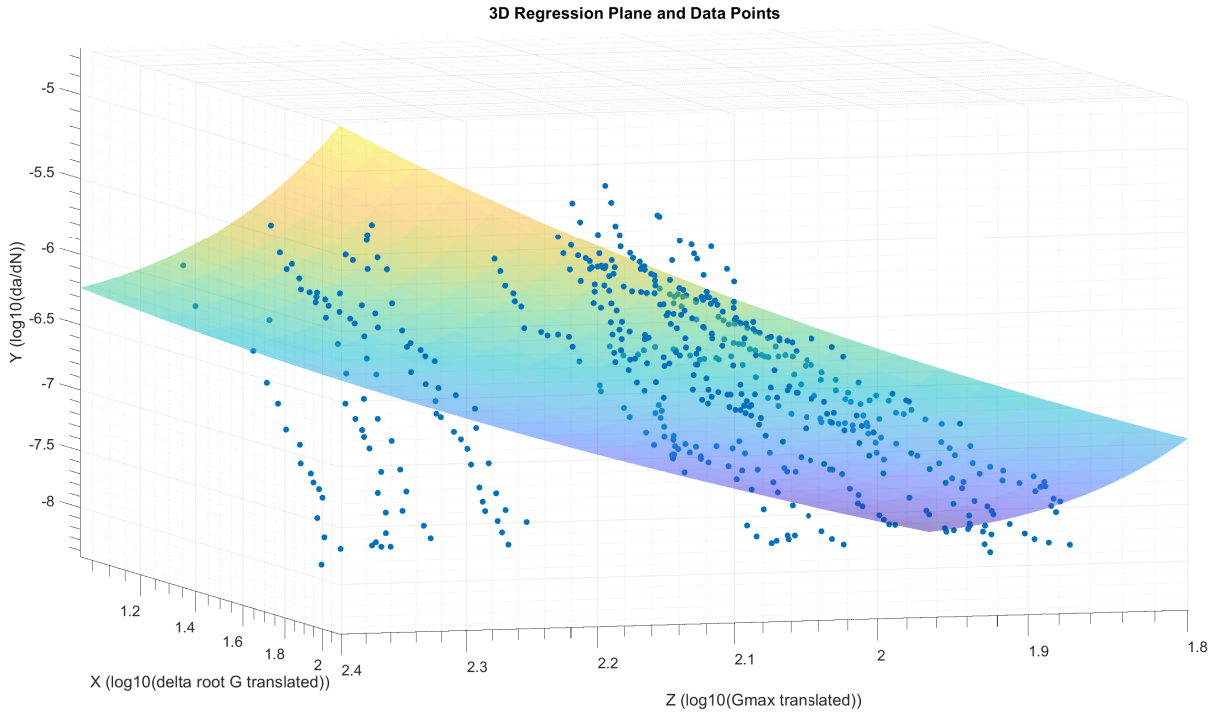

Figure A.4: Plane Fit using Regression of all the combined data